



HAL
open science

Sharp wave ripples during learning stabilize the hippocampal spatial map

Lisa Roux, Bo Hu, Ronny Eichler, Eran Stark, György Buzsáki

► **To cite this version:**

Lisa Roux, Bo Hu, Ronny Eichler, Eran Stark, György Buzsáki. Sharp wave ripples during learning stabilize the hippocampal spatial map. *Nature Neuroscience*, 2017, 20 (6), pp.845-853. 10.1038/nn.4543 . hal-03091338

HAL Id: hal-03091338

<https://hal.science/hal-03091338>

Submitted on 8 Jan 2021

HAL is a multi-disciplinary open access archive for the deposit and dissemination of scientific research documents, whether they are published or not. The documents may come from teaching and research institutions in France or abroad, or from public or private research centers.

L'archive ouverte pluridisciplinaire **HAL**, est destinée au dépôt et à la diffusion de documents scientifiques de niveau recherche, publiés ou non, émanant des établissements d'enseignement et de recherche français ou étrangers, des laboratoires publics ou privés.

Sharp wave ripples stabilize hippocampal spatial map during learning

Lisa Roux¹, Bo Hu^{1,4}, Ronny Eichler^{1,5}, Eran Stark^{1,6}, György Buzsáki^{1,2,3*}

¹New York University Neuroscience Institute, ²Department of Neurology, Medical Center and ³Center for Neural Science, New York University, New York, New York 10016, United States of America

⁴Third Military Medical University, College of Basic Medical Sciences, Department of Physiology, Chongqing, China

⁵Radboud University Nijmegen, Donders Centre for Neuroscience, Departments of Neuroinformatics and Neurophysiology, Nijmegen, Netherlands

⁶Tel Aviv University, Sackler Faculty of Medicine and Sagol School of Neuroscience, Department of Physiology and Pharmacology, Tel Aviv, Israel

*Corresponding author: gyorgy.buzsaki@nyumc.org

1 **ABSTRACT**

2

3 Cognitive representation of the environment requires a stable hippocampal map but the
4 mechanisms which secure map consistency are unknown. Because sharp wave-ripples
5 (SPW-R) assist in constructing both retrospective and prospective information, we
6 hypothesized that disrupting neuronal activity during SPW-Rs affects spatial
7 representation. Mice learned daily a new set of three goal locations on a multi-well maze.
8 We used closed-loop SPW-R detection at goal locations to trigger optogenetic silencing
9 of a subset of CA1 pyramidal neurons. Control place cells (non-silenced or silenced
10 outside SPW-Rs) largely maintained the location of their place fields after learning and
11 showed increased spatial information content. In contrast, the place fields of SPW-R-
12 silenced place cells remapped, and their spatial information remained unaltered. SPW-R
13 silencing did not impact the firing rates or the proportions of place cells. These results
14 indicate that SPW-R-associated activity during learning is instrumental for the
15 preservation and refinement of the hippocampal map.

16

17

18 **INTRODUCTION**

19

20 During exploration of an environment, hippocampal place cells fire selectively in
21 particular locations¹ (their “place fields”) and the sequential activation of groups of place
22 fields can reliably describe the trajectory of the animal². Collectively, a map-like
23 representation built from place cells may serve a cognitive navigation mechanism¹.
24 Remarkably, entire place cell sequences activated during exploration are repeated or
25 “replayed” during sharp wave ripple complexes (SPW-Rs), a network event observed in
26 the hippocampal local field potential³ during non-REM sleep⁴⁻⁷ and transient immobility
27 periods of waking exploration⁸⁻¹⁷. It has been hypothesized that SPW-R-related replay of
28 place cell sequences in the hippocampus mediates memory consolidation and transfer of
29 learned information from the hippocampus to the neocortex for long-term storage¹⁸⁻²⁰. In
30 support of this memory consolidation framework, experiments show that selectively
31 interfering with SPW-Rs during either sleep or waking deteriorates memory

32 performance^{15,21-23}. Awake SPW-Rs have also been shown to be involved in the planning
33 of future routes^{12,14,16,17}. More generally, SPW-Rs may have a “constructive” function,
34 establishing the cognitive maps of the physical world^{13,14,24,25}.

35

36 During learning and retrieval, memories are known to be transiently labile²⁶ and thus
37 require a subsequent stabilization process^{18,27}). If the neuronal mechanisms of mental
38 navigation and spatial navigation are indeed supported by similar neurophysiological
39 mechanisms²⁸, the question arises whether previously established spatial representations
40 also need to be “stabilized”. A recent experiment demonstrating that optogenetic
41 silencing of hippocampal neurons during exploration affects place field stability in a
42 familiar environment²⁹ suggests that it might be the case.

43

44 We hypothesized that SPW-Rs are instrumental in stabilizing the spatial representation
45 coded by place cells in the CA1 region of the hippocampus during learning. To examine
46 the role of SPW-Rs in place field stabilization, we used focal optogenetic silencing of a
47 subset of pyramidal neurons during SPW-Rs in a hippocampus-dependent spatial
48 memory task³⁰. The stability of the silenced place cells was compared with those of
49 simultaneously recorded but non-silenced place cells and place cells silenced after SPW-
50 Rs with a random delay. The spatial correlates of control place cells were largely
51 maintained and showed an increased information content after learning. In contrast, the
52 place fields of SPW-R-silenced neurons drifted and their information failed to increase.
53 Our findings thus establish that SPW-R-associated neuronal activity is necessary for
54 stabilizing and refining hippocampal place fields and, by extension, for maintaining a
55 stable cognitive map.

56

57

58 **RESULTS**

59

60 **Closed-loop focal optogenetic silencing of place cells**

61 Mice (n = 5; four CaMKII-Cre::Arch and one PV-Cre::ChR2; Supplementary Fig. 1)
62 were trained in a spatial learning task³⁰ (Fig. 1). After pre-training (3 to 4 days), they

63 were implanted with silicon probes in the CA1 region and recorded during free behavior
64 in their home cage or while performing on a “cheeseboard” maze. Mice carried two
65 LEDs (Fig. 1b), which allowed monitoring their exact location in real-time. Each session
66 consisted of five stages (Fig. 1a). During the learning epoch, the mouse performed
67 multiple trials (29 – 60 trials/session; median 50; n = 29 sessions; Supplementary Table
68 1) on the cheeseboard maze, where it had to find the locations of three goal wells (baited
69 with hidden water rewards) out of 177 possible wells. A trial was completed once the
70 mouse had retrieved all rewards and returned to the start box to collect an additional
71 water reward (Fig. 1c). The locations of the goal wells changed every day but were fixed
72 within a day. This strategy required the mice to daily update their memory for the new
73 goal locations in a familiar environment. Immediately before and after training, the
74 mouse was placed back in its home cage and allowed to sleep for approximately 1 h.
75 Memory performance and place field properties were assessed during pre- and post-
76 learning exploration epochs during which the mouse was allowed to explore the maze for
77 30 minutes. No rewards were available during the first 10 min, after which water drops
78 were placed in several randomly selected wells to encourage exploration of the entire
79 platform (online Methods). Similar to rats³⁰, daily learning was rapid, and the mice
80 developed stereotyped and efficient trajectories after 5-10 trials (Fig. 1c). Memory of the
81 newly learned goal locations was also demonstrated by the fact that mice spent
82 significantly more time at the goal locations during the first 10 minutes of the post-
83 learning epoch compared to pre-learning epoch (Fig. 1d; $P = 0.0006$; n = 29 sessions;
84 Wilcoxon’s paired signed rank test).

85

86 During the learning epoch of the task, SPW-Rs occurred regularly at the goal locations
87 while the animal was collecting rewards³⁰ (Fig. 2d). We hypothesized that these SPW-Rs
88 shape the spatial representation coded by place cells in this learning paradigm. To test the
89 impact of the SPW-Rs on CA1 hippocampal place fields, we used closed-loop
90 optogenetic silencing of pyramidal cells, contingent upon real-time detection of
91 spontaneous SPW-Rs at the goal locations. Importantly, optogenetic suppression of
92 pyramidal neuronal activity was conducted in a focal manner so that both light-
93 responsive and control neurons could be simultaneously recorded and compared, without

94 impacting the overall hippocampus function. In order to deliver light focally, the
95 recording silicon probes were equipped with etched optical fibers coupled to head-
96 mounted laser diodes (one fiber per shank; Fig. 2a-c) and implanted in one (n = 2) or both
97 (n = 3 mice) hemispheres. During the first rest period, we characterized the effect of light
98 on the firing rate of each recorded neuron (100 ms light pulses; 300 pulses at 0.2Hz; 204
99 $\pm 30 \mu\text{W}$, mean \pm SEM; online Methods). For each neuron, we defined a light-response
100 index by comparing spiking activity between the light pulses and the preceding baseline
101 periods (100ms intervals starting 1 s before stimuli onset) to define a light-response index
102 (Fig. 2c; online Methods). In both CaMKII-cre::Arch (direct suppression; Fig. 2b) and
103 PV-cre::ChR2 mice (indirect suppression; Supplementary Fig. 3), focal illumination
104 silenced most pyramidal cells recorded on the illuminated shank and occasionally some
105 on neighboring shanks (Fig. 2c). Of the 1020 putative pyramidal cells that we recorded,
106 402 of the were significantly suppressed ($P < 0.05$; Wilcoxon's paired signed rank tests;
107 online Methods).

108

109 During the learning epoch, light stimuli (60 ms pulses; same light intensity as during
110 response characterization) were triggered by online detection of spontaneous SPW-Rs to
111 focally suppress firing of pyramidal neurons and terminate SPW-R oscillations³¹ ("ripple-
112 locked" paradigm; Fig. 2d-e; n = 22 recording sessions). This SPW-R-contingent
113 silencing of pyramidal neurons was confined to events occurring when head of the mouse
114 was within the goal area by means of real time position tracking (Fig. 2d, green circles).
115 Our SPW-R manipulation was mild since light stimulation suppressed spiking mainly
116 during the second half of the SPW-Rs³¹. Yet, optogenetic stimulation was effective at
117 targeting most SPW-Rs during immobility periods ($82 \pm 4 \%$; online Methods). To test
118 for potential effects of light stimulation, not-specific to SPW-R silencing, light stimuli
119 were also delivered with a delay (100-300ms) relative to SPW-R detection ("ripple-
120 delayed" paradigm), either in separate recording sessions (n = 7 sessions) or in
121 combination with the ripple-locked paradigm but in the opposite hemisphere (n = 9
122 sessions). The behavioral performance (measured by the proportion of time spent in goal
123 areas in the post-learning exploration compared to the pre-learning exploration epoch; see
124 Fig. 1d) was identical regardless of whether a ripple-locked or a ripple-delayed paradigm

125 was employed during the learning task ($P = 0.75$; Mann-Whitney U test on the
126 differences Post - Pre; $n = 7$ ripple-delayed and $n = 13$ ripple-locked sessions).

127

128 Of the 1406 units recorded in 29 sessions, 227 were classified as putative interneurons
129 and 1020 as putative pyramidal cells (online Methods). Of the putative pyramidal cells,
130 637 had a place field on the cheeseboard maze in a least one of the two exploration
131 epochs (pre- and post-learning; online Methods). For quantitative analyses, we used two
132 approaches. (1) In the first approach, place cells that were silenced by light pulses in the
133 ripple-locked paradigm were referred to as *silenced*, whereas place cells silenced in the
134 ripple-delayed paradigm are referred to as *delayed*. Place cells that were unaffected by
135 light pulses in both of these stimulation paradigms were defined as *control* (Fig. 2f-g). Of
136 the 637 place cells, 106 were discarded because they did not meet our criteria for
137 classification (online Methods; Supplementary Table 1). Of the 531 remaining place
138 cells, 167 were assigned to the *silenced*, 81 to the *delayed* silenced and 283 the *control*
139 groups (Fig. 2g). (2) Because silencing of pyramidal neurons may bring about local
140 circuit effects³², we also used an alternative categorization, in which we grouped place
141 cells based on the type of intervention done (ripple-locked versus ripple-delayed
142 paradigms), independently of the magnitude of their responses to light. The two groups in
143 this second approach were referred to as *ripple-locked* and *ripple-delayed* place cells ($n =$
144 385 and $n = 247$ place cells, respectively).

145

146 **SPW-R-associated neuronal activity stabilizes place fields**

147 Stability of the hippocampal spatial map was examined by comparing recordings from
148 the pre-learning and post-learning exploration epochs in the *control*, *silenced* and *delayed*
149 groups of place cells. No light stimulation was administered during these epochs. Figure
150 3a-c illustrates representative rate maps for *control*, *silenced* and *delayed* place cells. For
151 each place cell, we calculated the pixel-by-pixel Pearson correlation coefficient between
152 the rate maps obtained from the pre- and post-learning epochs to quantify the stability of
153 the spatial representation. By comparing the resulting correlation coefficients across the
154 *control*, *silenced* and *delayed* groups, we found that optogenetic silencing of pyramidal
155 neurons during SPW-Rs reduced the stability of the rate map compared to control

156 neurons (Fig. 3d). In contrast, delayed suppression of place cells had no consistent effect
157 (mean correlation coefficient \pm SEM: 0.56 ± 0.02 ; 0.60 ± 0.03 and 0.49 ± 0.02 for
158 *control*, *delayed* and *silenced* ensembles, respectively; overall group effect, Kruskal
159 Wallis test, $P = 0.002$; Tukey's post-hoc tests, *silenced* vs *control*, $P = 0.008$; *silenced* vs
160 *delayed*, $P = 0.007$; *delayed* vs *control*, $P = 0.62$). We also quantified the proportion of
161 place cells which shifted their place fields so that their fields did not overlap between the
162 pre- and post-learning exploration epochs (Figure 3e; online Methods). The majority of
163 *control* and *delayed* silenced neurons preserved their place fields, as only a small fraction
164 of neurons (control group: 85/283, 30%; delayed group: 23/81, 24%) showed non-
165 overlapping place fields. In contrast, a larger fraction of neurons shifted their place
166 preference in the *silenced* group (75/167, 45%; $P = 5.8 \times 10^{-4}$, χ^2 test for 3 groups;
167 *silenced* vs *control*, $P = 0.004$; *silenced* vs *delayed*, $P = 0.04$; *delay* vs *control*, $P = 1$;
168 two-tailed Fisher's exact test with Bonferroni correction).

169

170 In the second approach, the pixel-by-pixel Pearson correlation between the rate maps
171 obtained from the pre- and post-learning exploration epochs was significantly different
172 between the *ripple-locked* and the *ripple-delayed* groups ($n = 385$ and $n = 247$ place cells,
173 respectively; $P = 0.007$; Mann-Whitney U test; Supplementary Fig. 7h). We found no
174 reliable correlation between the light response indices of individual place cells and their
175 stability, as assessed by the correlation coefficient of their pre- and post-learning rate
176 maps (Supplementary Fig. 7i). However, among the *ripple-locked* place cells, but not
177 among *ripple-delayed* neurons, those that switched their place field preference (no
178 overlapping place fields between pre and post-learning explorations) were more strongly
179 suppressed by light as compared to non-switching place cells (Supplementary Fig. 7k-l).
180 This result indicates that the most strongly suppressed cells in the *ripple-locked* group
181 showed the largest place field shifts. These findings show that suppressing neuronal
182 activity during SPW-Rs at the goal locations alters the place map of many place cells,
183 with the largest impact on the most strongly suppressed ones. Overall, this result further
184 confirms that activity during SPW-Rs is necessary for stabilizing place fields of
185 pyramidal neurons.

186

187 Importantly, differences in place field stability across the *silenced*, *control* and *delayed*
188 groups observed with the first approach could not be explained by mean or peak firing
189 rate differences, since these values did not differ across groups or between the pre-
190 learning and post-learning epochs (Supplementary Fig. 4b-c). One could also hypothesize
191 that SPW-Rs silencing would affect place field stability to the point that the silenced
192 neurons would lose their initial place fields and not even be classified as place cells in the
193 post-learning epoch. However, the three groups showed a similar proportion of neurons
194 that lost and gained place fields between the pre- and post-learning exploration epochs
195 (Supplementary Fig. 4e-f). Similarly, *ripple-locked* and *ripple-delayed* neurons defined
196 via the second approach did not differ in terms of firing rates or proportions of place cells
197 (Supplementary Fig. 7b-e). These observations indicate that although silenced individual
198 place cells change their spatial representation following SPW-R silencing, they still
199 effectively carry spatial information.

200

201 **SPW-R-triggered pyramidal cell silencing impairs place map refinement**

202 SPW-R silencing could also impact the amount of spatial information carried by place
203 cells. To explore this possibility, we compared the information content (bits/spikes)
204 carried by each place cell between the pre- and post-learning epochs (Fig. 4a-c). We
205 found that place cells in the *control* group carried more spatial information per spike in
206 the post-learning epoch compared to the pre-learning epoch (Fig. 4a ; $P = 0.007$,
207 Wilcoxon's paired signed rank test; $n = 283$). In contrast, information content of *silenced*
208 place cells did not increase significantly from pre-learning to post-learning epoch (Fig.
209 4c; $P = 0.86$; $n = 167$). Related measures of place field features followed a similar trend:
210 sparsity decreased and selectivity increased between the pre- and post-learning epochs in
211 the *control* group (sparsity, $P = 0.01$; selectivity, $P = 0.04$) . In contrast, these measures
212 remained unchanged in the *silenced* group (sparsity, $P = 0.97$; selectivity, $P = 0.44$).
213 Using the second approach, we confirmed that in the *ripple-delayed* (control) group,
214 spatial information per spike increased significantly in the post-learning exploration
215 epoch compared to the pre-learning epoch ($P = 0.00007$; $n = 247$; Wilcoxon's paired
216 signed rank test), whereas no difference was detected in the *ripple-locked* group ($P =$
217 0.49 ; $n = 385$; Supplementary Fig. 7f-g). Overall, these observations indicate that the

218 activity associated with SPW-Rs surrounding reward consumption contributes to the
219 refinement of the cognitive map coded by place cells.

220

221 **SPW-R-associated neuronal activity stabilizes place cell ensembles**

222 In the hippocampus, the representation of each spatial location relies on the coordinated
223 activity of multiple neurons². We thus tested whether optogenetic SPW-R-triggered
224 pyramidal cell silencing during learning impacts the stability of the spatial representation
225 at the population level, mirroring the effects we saw at the level of individual place cells.
226 The stability of the spatial representation coded by ensembles of place cells was
227 quantified by a population vector analysis^{30,33} (Fig. 5a). For each ensemble of
228 simultaneously recorded place cells (at least 5 place cells in each ensemble; range: 5-28),
229 the median correlation coefficient (computed across all pixels between the pre-
230 and post-learning exploration epochs) was defined to as a "stability score". This measure
231 provided an estimate of the consistency of the spatial representation at the neuronal
232 ensemble level (n = 24, n = 6, n = 16 ensembles for *control*, *delayed* and *silenced*
233 ensembles, respectively; Supplementary Table 1). Stability scores differed between the
234 three groups (stability scores : 0.68 ± 0.02 ; 0.72 ± 0.02 and 0.55 ± 0.03 for *control*,
235 *delayed* and *silenced* ensembles, respectively; P = 0.009; Kruskal Wallis test; Fig. 5e):
236 *silenced* assemblies showed a lower stability score than the *control* and *delayed*
237 ensembles (*post-hoc* Tukey's tests; P = 0.01, for *control* vs. *silenced*; P = 0.07 for
238 *delayed* vs. *silenced*; *control* vs. *delayed*: P = 0.94). Using the neuron assignment of the
239 second approach, we also observed a consistent difference between the stability scores of
240 *ripple-delayed* and *ripple-locked* place cell ensembles (P = 0.009; n = 19 *ripple-locked*
241 and 12 *ripple-delayed* ensembles; Mann-Whitney U test; Supplementary Fig. 7m-o).

242

243 To control for the possibility that the aforementioned ensemble destabilization effect of
244 SPW-R-triggered silencing was due to inter-session variability in the stability of place
245 cell ensembles, we performed within-session comparisons. On some recording days, we
246 recorded from sufficient numbers of neurons that allowed comparison between *silenced*
247 and *control* or *delayed* and *control* neurons ensembles in the same mouse (n = 15
248 sessions with *control* and *silenced* ensembles; n = 6 sessions with *control* and *delayed*

249 ensembles; Fig. 6a). In 12 of the 15 *control-silenced* sessions, the stability score was
250 higher in the *control* compared to the simultaneously-recorded *silenced* ensemble ($P =$
251 0.02 ; Wilcoxon's paired signed rank test) (Fig. 6b). In contrast, the *delayed* ensembles
252 showed both higher and lower stability scores than the simultaneously-recorded *control*
253 ensembles, and no group effect was observed ($P = 0.84$) (Fig. 6b). The stability score
254 differences between the pairs of simultaneously recorded ensembles was larger for
255 *control-silenced* pairs, compared to *control-delayed* pairs (Fig. 6c; $P = 0.05$; Mann-
256 Whitney U test). Similar results were obtained after controlling for ensemble size
257 (Supplementary Fig. 6, online Methods). These within-session differences between
258 control and manipulated place cell populations present further evidence that activity
259 during awake SPW-R promotes stabilization of place representation coded by
260 hippocampal neuron ensembles.

261

262

263 **DISCUSSION**

264

265 Our findings demonstrate that neuronal activity associated with SPW-Rs is critical for
266 maintaining place field stability in the hippocampal CA1 region. During each session,
267 place fields “stabilized” during the learning trials. Silencing pyramidal neurons during
268 SPW-Rs in the goal areas prevented them from becoming part of the stabilized map.
269 These results support the hypothesis that SPW-Rs promote the maintenance of the
270 cognitive map^{13,14,22,24}.

271

272 **Stabilization of the place map**

273 The stability of the cognitive map may deteriorate spontaneously or be modified by
274 various perturbations. Rats re-entering the same environment have been tacitly assumed
275 to have stable spatial maps^{1,34}. However, recent experiments suggest that the cognitive
276 map destabilizes over time^{33,35}. Moreover, firing rates and place field sizes undergo
277 changes during the first few trials, even after repeated exposure to the same familiar
278 environment³⁶. During these early trials the running speed is typically slow, the animal
279 often rears, scans the environments^{37,38} and stops frequently. SPW-Rs during such

280 immobility periods may be instrumental in maintaining the cognitive map^{14,24}. In our
281 experiments, distal environmental cues and the maze itself remained unchanged from day
282 to day and therefore, in principle, no novel construction of the spatial map was needed.
283 Yet, it is possible that learning and recalling the new reward locations contributed to a de-
284 stabilization of the hippocampal map³⁰, supporting the view that incorporating new
285 information in a pre-existing knowledge³⁹ (or "schema") necessitates a re-consolidation
286 process²⁷. Complementary to our findings, a recent experiment showed that global and
287 extended silencing of CA1 neurons during exploration affected place field stability²⁹.
288 Another relevant report showed that while individual place fields are present during the
289 first trials of daily sessions in a linear maze, stabilizing the relationship among place cell
290 assembly members requires several trials³⁸. Our experiments suggest neuronal activity
291 during SPW-Rs may play a critical role in this stabilization process.

292

293 The learning performance observed in mice was comparable to that of rats trained in a
294 similar task³⁰. However, in contrast to rats³⁰, we did not observe a reward-related
295 reorganization of place fields (Supplementary Fig. 8). The correlation maps obtained by
296 population vector analysis of SPW-R-silenced place cells did not show any consistent
297 spatial pattern with regards to reward locations or other locations in the maze (Fig 5 and
298 6). These observations suggest that SPW-R silencing did not impact the representation of
299 specific regions of the environment. Instead, representation of any location of the maze
300 had a similar chance to be affected. We therefore hypothesize that participation in SPW-
301 Rs contribute to the global maintenance of a singular map of the environment.

302

303 During exploration, two opposing classes of behaviors alternate: preparatory behaviors,
304 including locomotion of the animal from place to place (foraging), and consummatory
305 behaviors, including transient immobility and food/water consumption⁴⁰. These
306 respective behavioral classes are associated with theta and SPW-R patterns of the
307 hippocampus, respectively^{3,41}. One hypothesized role of consummatory states is to
308 maintain the cognitive map²⁸ and prepare the animal to calculate new routes in a familiar
309 environment^{24,42}. Similar to rats³⁰, SPW-Rs occurred regularly at reward locations when
310 the animal momentarily stopped and drank water. Aborting the buildup of SPW-Rs by

311 optogenetic means at the reward locations reduced place field stability tested across pre-
312 learning and post-learning exploration epochs. This was expressed by the reduced
313 correlation of place fields at both single neuron and population level, place field shifts,
314 spatial information content of spikes and related measures, without affecting their firing
315 rates. Importantly, our selective and focal optogenetic perturbations suppressed spiking in
316 only a small group of pyramidal cells with a minimal effect on neighboring networks
317 (Fig. 2c). Moreover, memory performance was similar whether the light stimulus was
318 presented during or after SPW-Rs. Therefore, it is unlikely that our optogenetic
319 manipulation exerted a major influence on the overall hippocampal computation. Instead,
320 our findings suggest that the small number of place cells silenced during SPW-Rs were
321 ‘left out’ from the ongoing map stabilization process.

322

323 **Mechanisms of SPW-R-assisted maintenance of place map**

324 In novel or changing environments, CA1 and CA3 neurons remap at different
325 rates^{30,33,43,44}). Notably, CA3 place fields are more stable than CA1 place fields across
326 repeated exposures to the same environment^{30,33,44}. Since CA3 constitutes the major drive
327 to CA1 during SPW-Rs³, SPW-Rs may be responsible for restoring a coherent
328 representation between CA3 and CA1 regions.

329

330 Alternatively, SPW-Rs may stabilize and refine CA1 place fields through a local impact
331 on CA1 circuits. Indeed, ample evidence suggests the importance of local processing
332 within the CA1 region. Whereas the CA3 drive can contribute to the sequential firing of
333 CA1 neurons during SPW-Rs, CA1 sequences can be also supported by local interactions
334 between pyramidal cells and interneurons⁴⁵, indicating CA3 input-independent
335 coordination in CA1 circuits. Local inhibition may shape the composition of cell
336 assemblies for specific regions of space^{29,32} and changes in interneuron networks have
337 been shown to mirror place field re-organization during learning in CA1⁴⁶. These
338 considerations suggest that the place map in CA1 is not simply inherited from upstream
339 regions but local processing contributes importantly to map stability.

340

341 Results from the ripple-delayed control group, demonstrate that transient optogenetic
342 hyperpolarization *per se* does not affect CA1 place fields. Indeed, we did not find
343 consistent differences between the non-light-modulated *control* and the *delayed* silenced
344 place cells in any stability measure. This control suggests that optogenetic
345 hyperpolarization does not induce a destabilization but rather *prevents* a stabilization
346 process to occur during SPW-Rs. The plasticity mechanisms associated with SPW-Rs
347 (that would support such stabilization) yet remain to be understood. During SPW-Rs,
348 spiking activity of CA1 neurons coincides with their organized CA3 inputs: dendritic
349 spikes may be induced and somadendritic backpropagation of spikes facilitated⁴⁷. The
350 coincidence of backpropagating spikes and the EPSCs evoked by the spike-inducing
351 inputs has been shown to induce synaptic plasticity⁴⁸. Dendritic subthreshold activity
352 during SPW-Rs could also support plasticity in the absence of somatic action
353 potentials^{49,50}. In our study, optogenetic hyperpolarization of pyramidal neurons during
354 SPW-Rs could have impacted these potential plasticity mechanisms preventing the
355 stabilization of the hippocampal map.

356

357 Overall, our observations suggest that SPW-Rs represent specific time windows during
358 which neurons engage in plasticity mechanisms essential for maintaining and refining the
359 cognitive map. These physiological findings demonstrate why it is beneficial that
360 ambulatory movements are interrupted by consummatory actions during exploration and
361 learning. Furthermore, they provide mechanistic insights into why SPW-R-related
362 activity supports memory function.

363

364 **Acknowledgments:**

365 We thank N. Chenouard, G. Girardeau, L. Sjulson, A. Peyrache and all members of the
366 lab for invaluable discussions, advice and comments on the manuscript. This work was
367 supported by NIH grants MH107396, MH54671, U01NS090583, the Simons Foundation
368 and the G. Harold and Leila Y. Mathers Foundation. L.R. was supported by the NIH
369 grant K99NS094735 and the Bettencourt Schueller Foundation. E.S. was supported by
370 the Rothschild Foundation, Human Frontiers in Science Program LT-000346/2009-L,

371 Machiah Foundation 20090098, and ERC-2015-StG 679253. B.H. was supported by the
372 National Natural Science Foundation of China (grant no. 31471050).

REFERENCES

1. O'Keefe, J. & Nadel, L. *Book The Hippocampus as a Cognitive Map.*, (Oxford University Press., 1978).
2. Wilson, M. A. & McNaughton, B. L. Dynamics of the hippocampal ensemble code for space. *Science* **261**, 1055-1058, (1993).
3. Buzsaki, G., Leung, L. W. & Vanderwolf, C. H. Cellular bases of hippocampal EEG in the behaving rat. *Brain Res* **287**, 139-171, (1983).
4. Wilson, M. A. & McNaughton, B. L. Reactivation of hippocampal ensemble memories during sleep. *Science* **265**, 676-679, (1994).
5. Kudrimoti, H. S., Barnes, C. A. & McNaughton, B. L. Reactivation of hippocampal cell assemblies: effects of behavioral state, experience, and EEG dynamics. *J Neurosci* **19**, 4090-4101, (1999).
6. Nadasdy, Z., Hirase, H., Czurko, A., Csicsvari, J. & Buzsaki, G. Replay and time compression of recurring spike sequences in the hippocampus. *J Neurosci* **19**, 9497-9507, (1999).
7. Lee, A. K. & Wilson, M. A. Memory of sequential experience in the hippocampus during slow wave sleep. *Neuron* **36**, 1183-1194, (2002).
8. Foster, D. J. & Wilson, M. A. Reverse replay of behavioural sequences in hippocampal place cells during the awake state. *Nature* **440**, 680-683, (2006).
9. Jackson, J. C., Johnson, A. & Redish, A. D. Hippocampal sharp waves and reactivation during awake states depend on repeated sequential experience. *J Neurosci* **26**, 12415-12426, (2006).
10. O'Neill, J., Senior, T. & Csicsvari, J. Place-selective firing of CA1 pyramidal cells during sharp wave/ripple network patterns in exploratory behavior. *Neuron* **49**, 143-155, (2006).
11. Csicsvari, J., O'Neill, J., Allen, K. & Senior, T. Place-selective firing contributes to the reverse-order reactivation of CA1 pyramidal cells during sharp waves in open-field exploration. *Eur J Neurosci* **26**, 704-716, (2007).
12. Diba, K. & Buzsaki, G. Forward and reverse hippocampal place-cell sequences during ripples. *Nat Neurosci* **10**, 1241-1242, (2007).
13. Karlsson, M. P. & Frank, L. M. Awake replay of remote experiences in the hippocampus. *Nat Neurosci* **12**, 913-918, (2009).
14. Gupta, A. S., van der Meer, M. A., Touretzky, D. S. & Redish, A. D. Hippocampal replay is not a simple function of experience. *Neuron* **65**, 695-705, (2010).
15. Jadhav, S. P., Kemere, C., German, P. W. & Frank, L. M. Awake hippocampal sharp-wave ripples support spatial memory. *Science* **336**, 1454-1458, (2012).
16. Pfeiffer, B. E. & Foster, D. J. Hippocampal place-cell sequences depict future paths to remembered goals. *Nature* **497**, 74-79, (2013).
17. Singer, A. C., Carr, M. F., Karlsson, M. P. & Frank, L. M. Hippocampal SWR activity predicts correct decisions during the initial learning of an alternation task. *Neuron* **77**, 1163-1173, (2013).
18. Buzsaki, G. Two-stage model of memory trace formation: a role for "noisy" brain states. *Neuroscience* **31**, 551-570, (1989).
19. Buzsaki, G. Hippocampal sharp wave-ripple: A cognitive biomarker for episodic memory and planning. *Hippocampus* **25**, 1073-1188, (2015).

20. Sutherland, G. R. & McNaughton, B. Memory trace reactivation in hippocampal and neocortical neuronal ensembles. *Curr Opin Neurobiol* **10**, 180-186, (2000).
21. Girardeau, G., Benchenane, K., Wiener, S. I., Buzsaki, G. & Zugaro, M. B. Selective suppression of hippocampal ripples impairs spatial memory. *Nat Neurosci* **12**, 1222-1223, (2009).
22. Nakashiba, T., Buhl, D. L., McHugh, T. J. & Tonegawa, S. Hippocampal CA3 output is crucial for ripple-associated reactivation and consolidation of memory. *Neuron* **62**, 781-787, (2009).
23. Ego-Stengel, V. & Wilson, M. A. Disruption of ripple-associated hippocampal activity during rest impairs spatial learning in the rat. *Hippocampus* **20**, 1-10, (2010).
24. Samsonovich, A. V. & Ascoli, G. A. A simple neural network model of the hippocampus suggesting its pathfinding role in episodic memory retrieval. *Learn Mem* **12**, 193-208, (2005).
25. Cheng, S. & Frank, L. M. New experiences enhance coordinated neural activity in the hippocampus. *Neuron* **57**, 303-313, (2008).
26. Nader, K., Schafe, G. E. & LeDoux, J. E. The labile nature of consolidation theory. *Nat Rev Neurosci* **1**, 216-219, (2000).
27. McKenzie, S. & Eichenbaum, H. Consolidation and reconsolidation: two lives of memories? *Neuron* **71**, 224-233, (2011).
28. Tolman, E. C. Cognitive maps in rats and men. *Psychol Rev* **55**, 189-208, (1948).
29. Schoenberger, P., O'Neill, J. & Csicsvari, J. Activity-dependent plasticity of hippocampal place maps. *Nat Commun* **7**, 11824, (2016).
30. Dupret, D., O'Neill, J., Pleydell-Bouverie, B. & Csicsvari, J. The reorganization and reactivation of hippocampal maps predict spatial memory performance. *Nat Neurosci* **13**, 995-1002, (2010).
31. Stark, E., Roux, L., Eichler, R., Senzai, Y., Royer, S. *et al.* Pyramidal cell-interneuron interactions underlie hippocampal ripple oscillations. *Neuron* **83**, 467-480, (2014).
32. Trouche, S., Perestenko, P. V., van de Ven, G. M., Bratley, C. T., McNamara, C. G. *et al.* Recoding a cocaine-place memory engram to a neutral engram in the hippocampus. *Nat Neurosci* **19**, 564-567, (2016).
33. Mankin, E. A., Sparks, F. T., Slayyeh, B., Sutherland, R. J., Leutgeb, S. *et al.* Neuronal code for extended time in the hippocampus. *Proc Natl Acad Sci U S A* **109**, 19462-19467, (2012).
34. Muller, R. U. & Kubie, J. L. The effects of changes in the environment on the spatial firing of hippocampal complex-spike cells. *J Neurosci* **7**, 1951-1968, (1987).
35. Ziv, Y., Burns, L. D., Cocker, E. D., Hamel, E. O., Ghosh, K. K. *et al.* Long-term dynamics of CA1 hippocampal place codes. *Nat Neurosci* **16**, 264-266, (2013).
36. Mehta, M. R., Barnes, C. A. & McNaughton, B. L. Experience-dependent, asymmetric expansion of hippocampal place fields. *Proc Natl Acad Sci U S A* **94**, 8918-8921, (1997).
37. Monaco, J. D., Rao, G., Roth, E. D. & Knierim, J. J. Attentive scanning behavior drives one-trial potentiation of hippocampal place fields. *Nat Neurosci* **17**, 725-731, (2014).

38. Feng, T., Silva, D. & Foster, D. J. Dissociation between the experience-dependent development of hippocampal theta sequences and single-trial phase precession. *J Neurosci* **35**, 4890-4902, (2015).
39. Tse, D., Langston, R. F., Kakeyama, M., Bethus, I., Spooner, P. A. *et al.* Schemas and memory consolidation. *Science* **316**, 76-82, (2007).
40. Woodworth, R. *Book Dynamic Psychology*. (Columbia University Press, 1918).
41. Vanderwolf, C. H. Hippocampal electrical activity and voluntary movement in the rat. *Electroencephalogr Clin Neurophysiol* **26**, 407-418, (1969).
42. Muller, R. U., Stead, M. & Pach, J. The hippocampus as a cognitive graph. *J Gen Physiol* **107**, 663-694, (1996).
43. Lee, I., Yoganarasimha, D., Rao, G. & Knierim, J. J. Comparison of population coherence of place cells in hippocampal subfields CA1 and CA3. *Nature* **430**, 456-459, (2004).
44. Kemere, C., Carr, M. F., Karlsson, M. P. & Frank, L. M. Rapid and continuous modulation of hippocampal network state during exploration of new places. *PLoS One* **8**, e73114, (2013).
45. Stark, E., Roux, L., Eichler, R. & Buzsaki, G. Local generation of multineuronal spike sequences in the hippocampal CA1 region. *Proc Natl Acad Sci U S A* **112**, 10521-10526, (2015).
46. Dupret, D., O'Neill, J. & Csicsvari, J. Dynamic reconfiguration of hippocampal interneuron circuits during spatial learning. *Neuron* **78**, 166-180, (2013).
47. Kamondi, A., Acsady, L. & Buzsaki, G. Dendritic spikes are enhanced by cooperative network activity in the intact hippocampus. *J Neurosci* **18**, 3919-3928, (1998).
48. Magee, J., Hoffman, D., Colbert, C. & Johnston, D. Electrical and calcium signaling in dendrites of hippocampal pyramidal neurons. *Annu Rev Physiol* **60**, 327-346, (1998).
49. Golding, N. L., Staff, N. P. & Spruston, N. Dendritic spikes as a mechanism for cooperative long-term potentiation. *Nature* **418**, 326-331, (2002).
50. Bittner, K. C., Grienberger, C., Vaidya, S. P., Milstein, A. D., Macklin, J. J. *et al.* Conjunctive input processing drives feature selectivity in hippocampal CA1 neurons. *Nat Neurosci* **18**, 1133-1142, (2015).

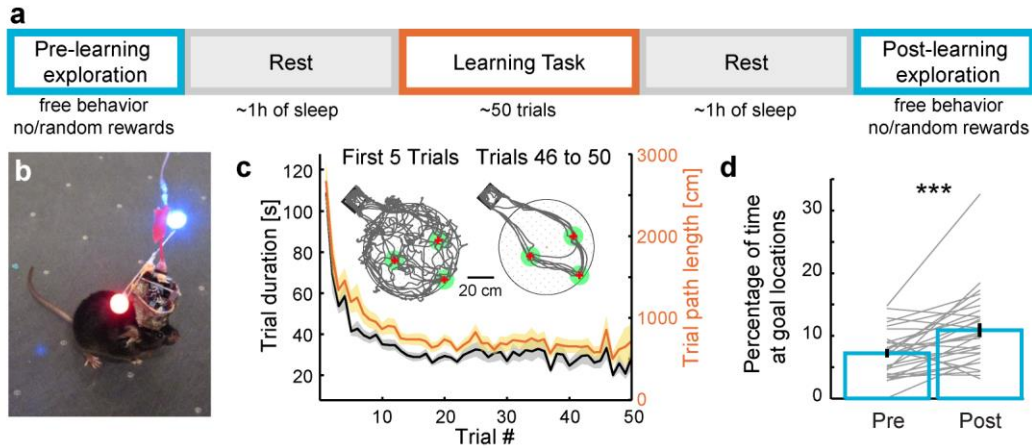


Figure 1: Daily spatial learning of hidden reward locations on the cheeseboard maze. **(a)** Five steps constituting a daily recording session³⁰: (1) pre-learning exploration epoch, (2) rest epoch in home cage, (3) learning task, (4) rest epoch in home cage and (5) post-learning exploration epoch. **(b)** Implanted mouse equipped with blue and red LEDs allowing real-time position tracking. **(c)** Learning performance during the task. A new set of three baited wells was randomly selected every day but stayed fixed within a given day. Lines with shaded areas show mean \pm SEM for $n = 29$ sessions in 5 mice. **(d)** Mice spent consistently more time at the goal locations during the first 10 min of the post-learning exploration epoch, compared to the first 10 min of the pre-learning exploration epoch (7 ± 0.007 and 11 ± 0.01 % of the time for pre and post, respectively; *** $P = 0.0006$, Wilcoxon's paired signed rank test, $n = 29$ sessions in 5 mice).

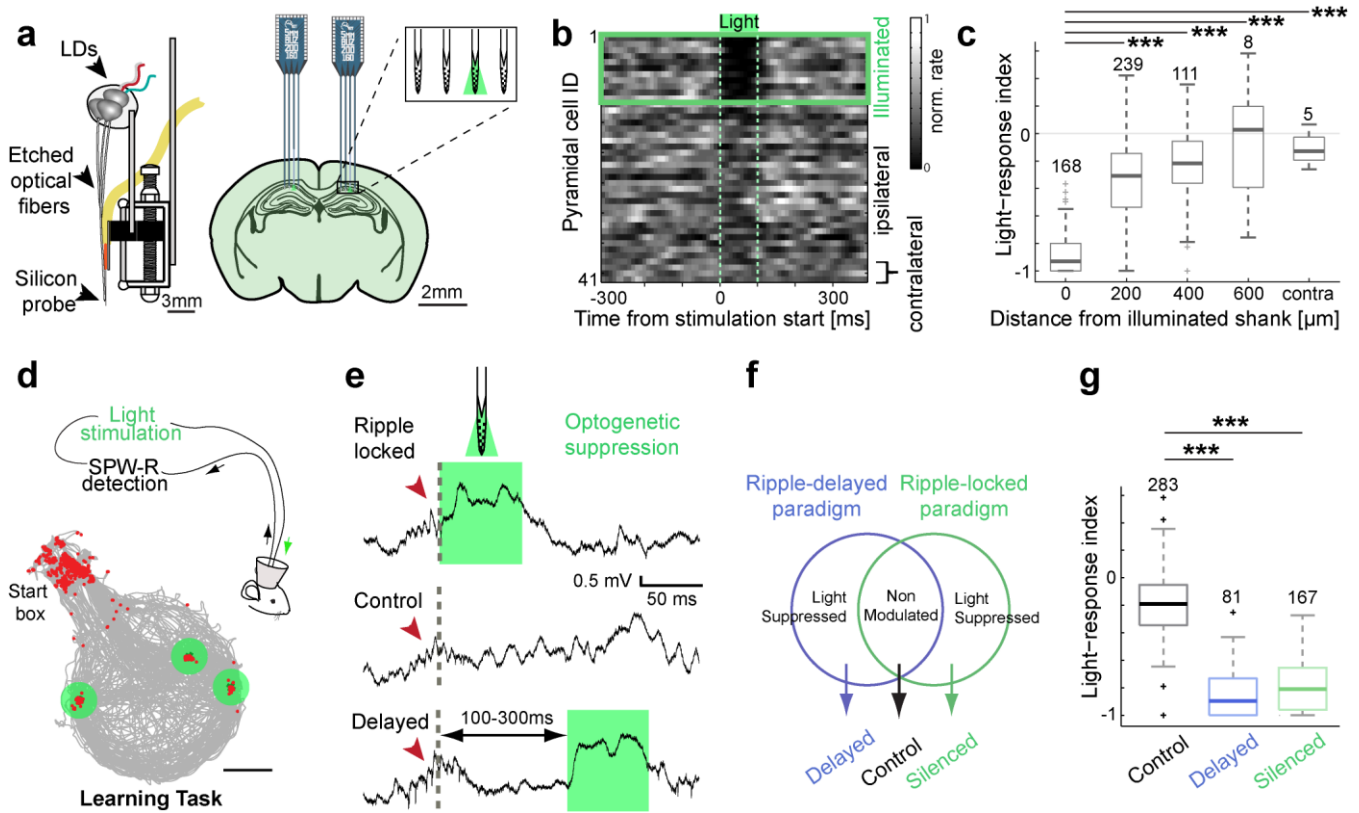


Figure 2: Closed-loop focal optogenetic silencing of pyramidal cells contingent upon SPW-R detection at goal locations. **(a)** Left: Schematic of a diode-probe mounted on a movable drive. Right: Diode-probes were implanted uni- or bilaterally in the dorsal CA1 hippocampal region. **(b)** Peristimulus histogram for a population of simultaneously recorded pyramidal cells, illustrating the local silencing effect provided by focal light delivery: units recorded on the illuminated shank (top; green box) are strongly suppressed during illumination. **(c)** Light response indices as a function of distance from illuminated shank. The number of cells recorded at each distance is shown above boxes. Indices: -0.88 ± 0.01 ($0 \mu\text{m}$), -0.34 ± 0.02 ($200 \mu\text{m}$); -0.24 ± 0.02 ($400 \mu\text{m}$); -0.06 ± 0.15 ($600 \mu\text{m}$); -0.11 ± 0.05 (contralateral hemisphere). Kruskal Wallis test: $***P = 2.4 \times 10^{-64}$; Tukey's *post-hoc* tests: $***P < 0.001$ for comparisons between neurons from illuminated shank versus other neurons; $P > 0.05$ for all other comparisons; $n = 531$ place cells. **(d)** Offline detected SPW-Rs (red dots) are displayed on top of the animal trajectory (gray) for an example learning session. Note that SPW-Rs mainly occur at the goal locations

(green disks) and in the start box. Light stimuli (60ms) were triggered by SPW-Rs in the goal areas. **(e)** Light stimuli aborted ripples locally (top) but had no effect in the control (non-illuminated shank, middle) and delayed (bottom) condition. **(f)** Schematic illustrating place cell classification into three categories based on experimental paradigm (optogenetic stimulation triggered with or without delay relative to SPW-R detection) and their firing rate modulation by light (see online Methods). **(g)** Optogenetic silencing effect in the three groups of place cells. Indices: -0.20 ± 0.01 (*control*), -0.84 ± 0.02 (*delayed*); -0.78 ± 0.02 (*silenced*). Kruskal Wallis test: $***P = 2.6 \times 10^{-78}$; Tukey's *post-hoc* tests, $***P < 0.001$; $n = 283, 81, 167$ *control, delayed* and *silenced* place cells.

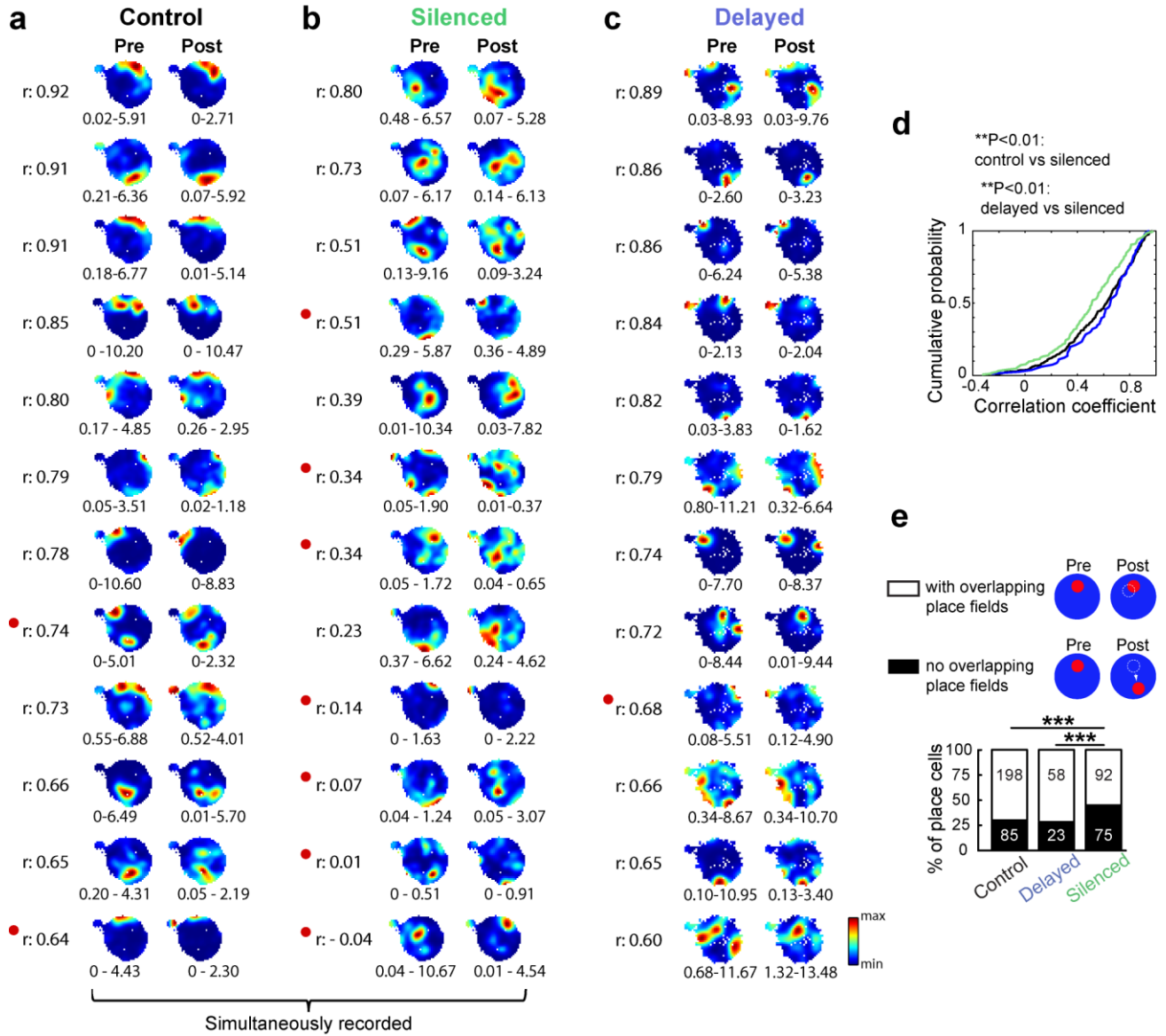


Figure 3: Silencing neurons during SPW-Rs impairs place map stability of place cells. **(a-c)** Examples of firing rate maps obtained from the pre- and post-learning exploration epochs in example sessions for individual *control* **(a)**, *silenced* **(b)** and *delayed* **(c)** place cells. The correlation coefficient (r), calculated by comparing firing rate maps in pre and post-learning exploration epochs, is shown for each place cell on the left. Red dots indicate shifting place fields (“no overlapping place fields” as in **e**). Twelve place cells in with the highest r values in each category are depicted. Control and silenced place cells (**a** and **b**) were recorded during the same session. **(d)** Cumulative distributions of the r values obtained for individual place cells in the three groups. Kruskal Wallis test: **P =

0.002; Tukey's *post-hoc* tests: **P = 0.008 (control vs silenced), **P = 0.007 (delayed vs silenced), P = 0.62 (control vs delayed); n = 283 control, n = 81 delayed and n = 167 SPW-R silenced place cells. **(e)** Proportions of place cells with shifting fields (no overlapping place fields, black) or overlapping place fields (white) in the three groups of place cells. The number of cells in each category is indicated on the bars. χ^2 test: ***P = 5.8×10^{-4} ; *post-hoc* two-sided Fisher's exact tests followed by Bonferroni correction: **P = 0.004 (control vs silenced), *P = 0.04 (delayed vs silenced), P = 1 (control vs delayed).

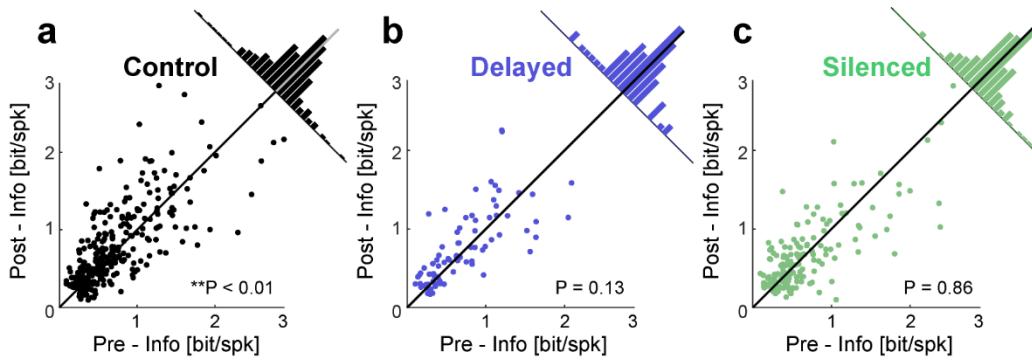


Figure 4: SPW-R silencing impact information measures of place cells. **(a-c)** Distributions of “information content” values carried by place cells during pre- and post-learning exploration epochs. The information content of *silenced* place cells (c) remained similar across pre- and post-learning exploration epochs (0.68 ± 0.04 and 0.67 ± 0.04 bit/spk for pre and post, respectively; Wilcoxon’s paired signed rank test: $P = 0.86$; $n = 167$ SPW-R *silenced* place cells) while *control* place cells (a) showed an increased information content (*control* group: 0.74 ± 0.03 and 0.80 ± 0.03 bit/spk for pre and post, respectively; *delayed* group: 0.70 ± 0.05 and 0.75 ± 0.05 bit/spk; $P = 0.007$, $P = 0.13$ for *control* and *delayed* groups, respectively; $n = 283$ control, $n = 81$ delayed silenced place cells). Two outlier values in the *silenced* and *control* groups are not displayed but included in the statistical analyses (their exclusion does not affect the conclusions).

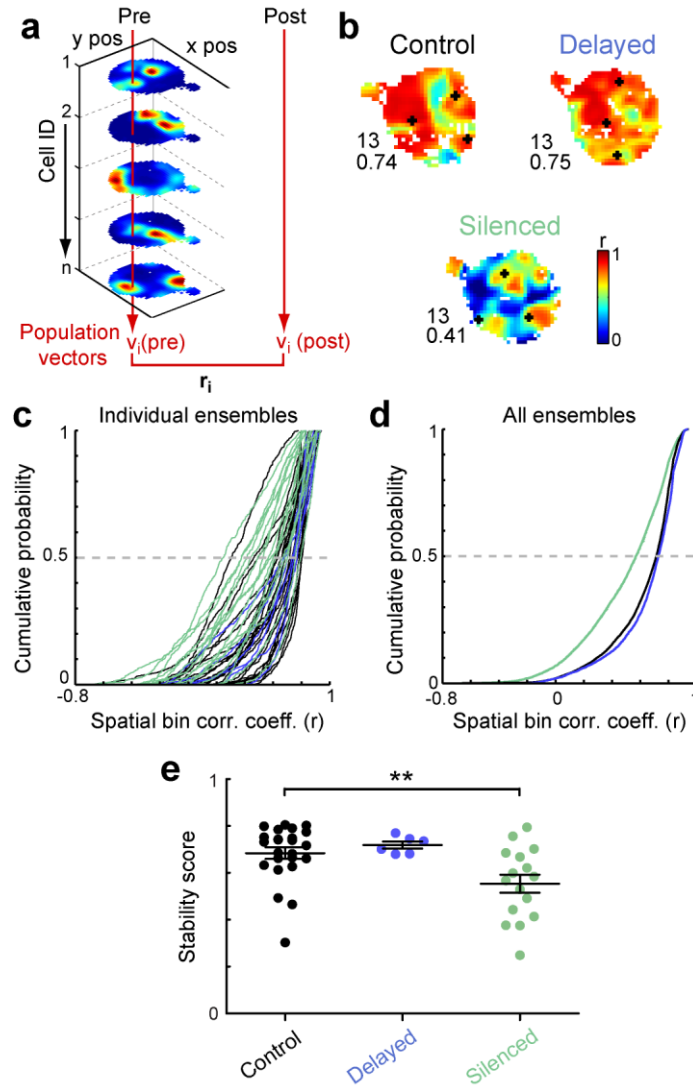


Figure 5: Silencing neurons during SPW-Rs impairs place map stability of place cell ensembles. **(a)** Schematic illustrating population vector analysis method. For each spatial bin i , a population vector v_i was constructed containing the rates in the bin i of each cell of the ensemble. This was done for all spatial bins, separately for the rate maps of the pre- and post-learning exploration epochs. Then, for each spatial bin i , the Pearson correlation (r_i) between $v_i(\text{pre})$ and $v_i(\text{post})$ was computed. r_i indicates the stability of the ensemble spatial representation at pixel i . Correlation maps were constructed by assigning the r values to their respective positions in x and y . **(b)** Examples of correlation maps obtained for ensembles of *control*, *delayed* and *silenced* place cells. Correlation

values of individual spatial bins (r) are color coded. The number of cells part of the ensemble and the stability score, defined as the median of all bins' correlation values (r), are indicated on the left of each map. Goal locations are indicated by black crosses. **(c)** Cumulative distribution of population correlation values across spatial bins for individual ensembles of place cells. $n = 24$ *control* (black), 6 *delayed* (blue) and 16 *silenced* ensembles of place cells (green). **(d)** Cumulative distributions of the correlation values accumulated for all ensembles of place cells from the three groups. **(e)** Stability scores for the individual ensembles of place cells shown in (c). Kruskal Wallis test: $**P = 0.009$; Tukey's *post-hoc* tests: $*P = 0.013$ (control *vs* silenced), $P = 0.94$ (control *vs* delayed), $P = 0.068$ (delayed *vs* silenced).

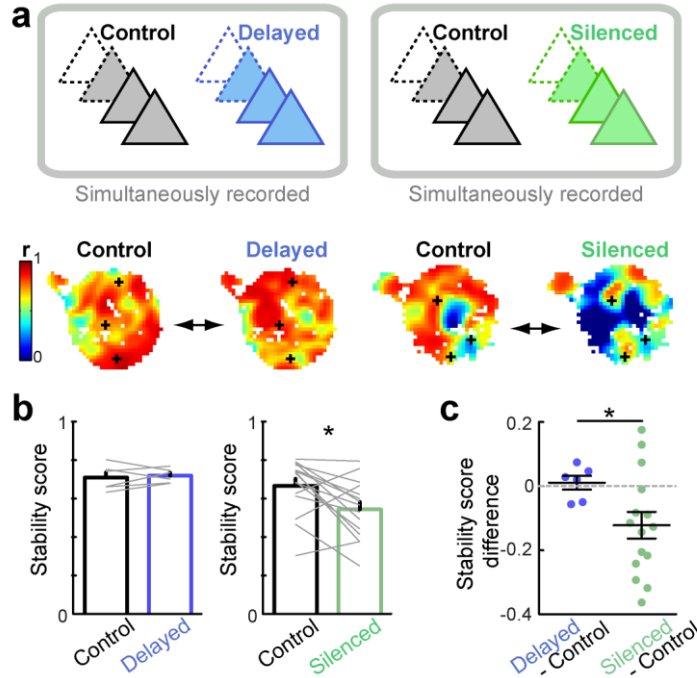


Figure 6: SPW-R silenced ensembles of place cells show destabilized spatial representation as compared to simultaneously recorded control ensembles. **(a)** Top: Schematic illustrating the method used for within-session comparison of place cell ensemble pairs. Bottom: Examples of correlation maps for pairs of ensembles, simultaneously recorded within the same session (left, ensembles of *control* and *delayed* place cells; right, ensembles of *control* and *silenced* place cells) **(b)** Left: Ensembles of *delayed* place cells show similar stability scores to their matched *control* from the same recording session (score: 0.71 ± 0.03 and 0.72 ± 0.02 for *control* and *delayed* ensembles, respectively; Wilcoxon's paired signed rank test: $P = 0.84$, $n = 6$ pairs). Right: In contrast, ensembles of *silenced* place cells show a lower stability score compared to their matched *control* ensembles (score: 0.67 ± 0.04 and 0.54 ± 0.04 for *control* and *silenced* ensembles, respectively; $*P = 0.015$, $n = 15$ pairs). **(c)** Within-session differences between the stability scores of optogenetically manipulated ensembles and their matched control ensembles (0.01 ± 0.02 for *delayed-control* pairs and -0.12 ± 0.04 for *silenced-control* pairs). Mann-Whitney U test: $*P = 0.047$. Dashed grey line indicates zero level (no difference).

1 **Online Methods:**

2

3 **Subjects and electrode implantation**

4 All experiments were approved by the Institutional Animal Care and Use Committee of New
5 York University Medical Center. We used transgenic mice to obtain expression of exogenous
6 light-sensitive opsins⁵³: four mice expressed archaerhodopsin-3⁵⁴ (“Arch”) under control of the
7 pyramidal cell selective calcium/calmodulin-dependent protein kinase II alpha - CaMKIIalpha
8 - promoter (referred to as CaMKII-cre::Arch) and one mouse expressed channelrhodopsin-2⁵⁵
9 (“ChR2”) under the parvalbumin - PV - promoter, primarily expressed in a subpopulation of
10 inhibitory interneurons (referred to as PV-cre::ChR2; Supplementary Fig. 3, Supplementary
11 Table 1). These mice were obtained by breeding the cre-dependent “responder” lines
12 expressing Arch (Ai35D allele; Jackson stock no. 012735) and ChR2 (Ai32 allele; Jackson
13 stock no. 024109) with the “driver” lines expressing the Cre recombinase under the
14 CaMKIIalpha⁵⁶ (Jackson stock no. 005359) and PV⁵⁷ (Jackson stock no. 008069) promoters.
15 These five adult male mice (3-5 months old) were implanted unilaterally or bilaterally with
16 high-density silicon probes (32 or 64 sites; Buz32 or Buz64; NeuroNexus), attached to
17 movable microdrives (Fig. 1a), under isoflurane anesthesia, as described previously⁵¹. In all
18 experiments, ground and reference screws were implanted in the bone above the cerebellum.
19 Probes were implanted perpendicularly to the midline, or with a 45-degree angle along the
20 hippocampal long axis, at the following coordinates: AP: -1.7 mm; ML: +1 or -1 mm (left or
21 right hemisphere). Two mice were implanted at AP: - 1.8, ML: +/- 1.4. During surgery, the tips
22 of the probes were lowered to the neocortex (depth: 700 μ m). After 4–7 d of recovery, they
23 were moved gradually (≤ 70 μ m/day) until reaching the CA1 pyramidal cell layer of the dorsal
24 hippocampus, characterized by large amplitude ripple oscillations. Neuronal spiking activity
25 and LFP were recorded daily in the behavioral task (Fig. 1a) and the position of the probe was
26 optimized at the end of each daily session to obtain the maximal unit yield. The composition of
27 spiking population varied from session to session due to either active movement of the probe or
28 to spontaneous movement of the brain tissue. We cannot exclude some overlap between the
29 units recorded in the different sessions from the same animal. However, this was not
30 considered as an issue since from day to day, we varied the positions of the rewards on the

31 maze (new learning), and other parameters such as the type of light stimulation (with or
32 without delay), and the identity of the illuminated shanks (for mice with multiple diodes). At
33 the end of the experiment, the mice were perfused and the electrode locations were verified by
34 histology.

35

36 **Diode-probes**

37 The probes consisted of 4 or 8 shanks (200- μm shank separation) and each shank had 8
38 recording sites (160 μm^2 each site, 1–3-M Ω impedance), staggered to provide a two-
39 dimensional arrangement (20- μm vertical separation) (Buz32 or Buz64; NeuroNexus). One or
40 more multimode optical fibers (core diameter: 50 μm) were attached to the probe shanks,
41 terminating in a tip etched to a point above electrode sites. At the other end, fibers were
42 coupled to laser diodes⁵¹ (450 nm blue laser diode for ChR2 activation; 639 nm red laser diode
43 or 520 nm green laser diode for Arch activation) (Fig. 2a). Peak light power, measured at the
44 tip of the shanks before implantation, was: 191 \pm 11 μW (mean \pm SEM; n = 2 blue laser diodes),
45 320 \pm 73 μW (n = 3 red laser diodes) and 151 \pm 19 μW (n = 6 green laser diodes).

46

47 **Data acquisition**

48 During the recording session, neurophysiological signals were acquired continuously at 20 kHz
49 on a 256-channel Amplipex system (Szeged, Hungary; 14-bit resolution, analog
50 multiplexing)⁵⁸. The wide-band signal was downsampled to 1.25 kHz and used as the LFP
51 signal. A three-axis accelerometer (ADXL-330, Analog Devices) was attached to the signal
52 multiplexing headstage for monitoring movements. For tracking the position of the mouse on
53 the cheeseboard maze and in its home cage, two small light-emitting diodes, mounted above
54 the headstage, were recorded by a digital video camera at 30 frames/s. The LED locations were
55 detected and recorded online with a custom-made tracking software.

56

57 **Pre-training**

58 All mice were free from prior manipulation before being included in this study and were
59 maintained on a 12h:12h light-dark cycle (lights on at 07:00 a.m.) in the vivarium (maximum 5

60 adult mice per cage; housed individually after surgery). Before electrode implantation, the
61 mice were handled daily for at least one week and pre-trained on the spatial learning task on
62 the cheeseboard maze. All experiments were done during the day (light-cycle). Pre-training
63 consisted first in simple exposure to the platform and the start box, 1 hour daily, during two
64 days while water deprivation started. On the two following days, the mouse was allowed to
65 collect ~20 water rewards (10 μ L each) placed in the wells at random locations on the maze.
66 On subsequent days, the animal was trained to locate three water rewards per trial (see below).
67 No probe test was conducted during pre-training. Pre-training was completed when the mouse
68 was able to perform at least 20 trials per session (3 to 4 days). It was then allowed to recover
69 from water deprivation and regain full weight.

70

71 **Behavioral training**

72 Mice were trained to perform a spatial learning task on a cheeseboard maze, similarly to the
73 task previously described for rats^{30,59}. The maze consisted of a circular platform 80 cm in
74 diameter with 177 wells (1.5 mm deep; 4 mm in diameter; 5 cm spacing between the wells)
75 and a start box placed next to the platform (Fig. 2d). Access to the platform from the start box,
76 and to the start box from the platform, was controlled by a manually operated door. Each daily
77 session consisted of five epochs during which hippocampal activity and behavior were
78 continuously recorded: (1) a pre-learning exploration epoch, (2) a rest epoch, (3) a learning
79 task, (4) a rest epoch and (5) a post-learning exploration epoch (Fig.1a). For the two rest
80 epochs, the animal was returned to its home cage and allowed to sleep for ~1 hour. The mouse
81 was exposed to the cheeseboard maze during the two exploration epochs and the learning task.
82 During the learning task, mice learned the locations of three hidden water rewards (5 μ L) on
83 the cheeseboard maze, out of 177 possible wells (Fig.1c). A new set of three baited wells was
84 randomly selected every day but stayed fixed within a given day. A trial was completed once
85 the mouse had retrieved the three rewards and returned to the start box (median: 50 trials;
86 range: 29 – 60 trials; n = 29 sessions, 5 mice). Access to the start box was conditioned upon
87 successful retrieval of the three baits. However, a trial was aborted and the animal was allowed
88 to return to the start box in the rare cases when the three water rewards were not collected
89 within 4 minutes (from trial start). To prevent the possible use of an odor-guided search

90 strategy that could interfere with spatial learning, the cheeseboard platform was rotated relative
91 to the start box between trials. In addition, the maze was wiped after every 5 trials and at the
92 end of each pre- and post-learning exploration epochs with a tissue paper soaked in alcohol.
93 Thus, goal locations were defined in an extra-maze reference frame. Each exploration epoch
94 was divided into three blocks of 10 minutes. In the first block, no reward was presented and the
95 animal was allowed to freely explore the platform. In the two following blocks, the mouse was
96 provided with five water rewards at randomly selected locations (different locations for the two
97 blocks, but same locations for the pre and post-learning explorations). The mouse was allowed
98 to return to the start box between each block. This strategy was used to promote complete
99 spatial exploration of the platform, a necessary condition to study the spatial information coded
100 by hippocampal assemblies. To quantify memory performance after learning, only the first
101 block of each pre/post-learning exploration epoch was considered. Memory performance was
102 assessed by calculating the proportion of time the mouse spent in the goal areas (15 cm
103 diameter circular regions centered on goal locations) relative to the block duration (10 min) in
104 the pre- and post-learning exploration epochs (Fig.1d). When comparing learning performance
105 in ripple-delayed and ripple-locked paradigms, only sessions where a single type of paradigm
106 was delivered during learning were considered (i.e., we excluded sessions where both ripple-
107 locked and ripple-delayed stimulations were used in different hemispheres). Learning
108 performance during the learning task was assessed by the distance traveled to retrieve the
109 rewards during each trial or the time it took for the mouse to collect the three rewards (Fig. 1c).

110

111 **Unit clustering and neuron classification**

112 Spikes were extracted from the high-pass filtered signals (median filter, cutoff frequency: 800
113 Hz) offline, the waveforms were projected onto a common basis obtained by principal
114 component analysis (PCA) of the data, and sorted into single units automatically using
115 KlustaKwik⁶⁰ followed by manual adjustment using the software Klusters⁶¹
116 (<http://neurosuite.sourceforge.net/>). For each unit, the single recording site with the maximal
117 trough amplitude mean waveform was selected and two waveform features were computed: the
118 trough-to-peak and the spike width (the inverse peak frequency of the spike spectrum,
119 estimated by 1024-point FFT of the zero-padded waveforms). This generated two clearly

120 separable clusters (Supplementary Fig. 2a). Putative pyramidal (PYR) and interneurons (INT)
121 were identified based on a Gaussian-mixture model using these two waveform features⁵². This
122 model was previously built on the waveforms of optogenetically tagged neurons, and neurons
123 showing mono-synaptic connections in the hippocampal CA1 region. It enabled assigning a P-
124 value to the classification of each unit and units with low classification confidence ($p > 0.05$)
125 were discarded (21/1406 units, 1.5%). When the identity of a unit defined by this method was
126 considered ambiguous, it was also excluded from the analysis (138/1406 units, 9.8%).
127 Classification of units as PYR and INT was done blindly, i.e., without a priori knowledge of
128 the group the unit belonged to (*control*, *delayed* or *silenced*). We recorded a total of 1406 well-
129 isolated units from CA1 of 5 freely-moving mice in 29 sessions (Supplementary Table 1). Of
130 these, 1020 were putative pyramidal cells and 227 were putative interneurons. 159 well-
131 isolated units were not classified.

132

133 **Optogenetic suppression of pyramidal neurons**

134 The response of each recorded unit to light was tested with a series of light pulses applied
135 during the first rest epoch of each daily recording session (~ 300 pulses per LD, 100 ms each,
136 one pulse every 5 s). This response mapping procedure allowed us to compare the firing rate of
137 each unit before (baseline) and during the light pulses (baseline: 100 ms intervals starting 1 s
138 before each stimulus onset). A unit was considered light-suppressed when the mean firing rates
139 during the light pulses (R_{light}) were significantly reduced as compared to baseline activity
140 (R_{baseline}) ($P < 0.05$, Wilcoxon's signed-rank test for matched values, one-tailed test). We
141 computed the light-response index for each unit according to the following formula:

$$142 \text{ Light-response index} = (R_{\text{light}} - R_{\text{baseline}}) / (R_{\text{light}} + R_{\text{baseline}})$$

143 An index of value “zero” indicates no change as compared to baseline; “negative one”
144 indicates complete silencing. In case of bilateral light delivery and recording, only the response
145 to the light stimulus delivered ipsilaterally to the recorded cell was considered. Units classified
146 as *control* included non-significantly modulated neurons (neither suppressed, nor excited
147 during light pulses; $P > 0.05$, Wilcoxon's signed rank tests) recorded exclusively from non-
148 illuminated shanks (Fig. 2f-g). Of the 1020 recorded putative pyramidal cells, 141 were
149 excluded because they were not identified as light-responsive and were located on illuminated

150 shanks (excluded control cells) or showed an increased activity during light pulses. A neuron
151 was also discarded if its baseline firing rate was too low to determine whether a spike count of
152 zero during light pulses was distinct from the spike count expected by chance. Assuming a
153 Poisson distribution of the neuron spike counts, the minimal (expected) number of spikes
154 during the total light pulse duration (λ) that could, simply by chance, result in zero spikes
155 is 3 for an alpha level of 0.05. Therefore, with 30 s of response mapping light pulses (300
156 pulses of 100 ms), cells that fired less than 0.1 spikes/s during baseline were excluded (17
157 pyramidal cells out of 1020). Of the remaining putative pyramidal cells, 273 units were
158 silenced by SPW-R-triggered light pulses, 129 units were silenced with a delay (100-300 ms
159 following SPW-R detection) and 460 served as control units.

160

161 **SPW-R-triggered closed-loop light stimulation**

162 A single channel from the middle of the CA1 pyramidal cell layer with the largest amplitude
163 ripple was selected for real-time processing of LFP by a programmable digital signal processor
164 (DSP) running at 25 kHz (RX6, Tucker-Davis Technologies). The root-mean-square (RMS) of
165 the band-pass filtered (80-250 Hz) signal was computed in two running windows, long (2 s;
166 RMS1) and short (8 ms; RMS2). Ripples were defined as events with RMS2 exceeding three
167 times RMS1 (range: 3-3.5) for at least 8 ms³¹. Light stimuli (60 ms square pulses) were applied
168 in a closed-loop manner during the learning task, exclusively when the mouse was located at
169 the reward locations (15 cm diameter circular areas centered on the three baited wells) (Fig.
170 2d). This spatially-conditioned stimulation was achieved using a custom tracking software
171 which detected, in real time, the periods when the mouse was located within the pre-defined
172 goal areas. As a control, delayed stimuli (60 ms pulses) were presented at random intervals
173 between 100 and 300 ms following SPW-R detection.

174 In order to quantify the effectiveness of the online SPW-R detection, we used the first 3 min of
175 the post-learning epoch when the online detection was conducted but no light stimulus was
176 delivered. During this period, the mouse was in the start box before being released for
177 exploration. SPW-Rs that occurred during immobility periods ($< 3\text{cm/s}$ movement) were
178 visually identified in each session blindly (without the knowledge of online detection) and
179 subsequently compared to the online detections. Overall, $83 \pm 4\%$ of the visually identified

180 SPW-Rs were detected by the online detection program (n = 17 sessions). The SPW-Rs missed
181 by online detection were typically of smaller amplitude events and shorter in duration as
182 compared to online-detected SPW-Rs. Conversely, $63 \pm 4\%$ of all online detected SPW-Rs
183 were considered as ‘false positive’ events by the visual scoring. These false positive events
184 were typically due to muscle artifacts or large power fast gamma events during small
185 movements. These falsely detected SPW-Rs necessitated the inclusion of delayed-stimulation
186 control experiments.

187

188 **Spatial tuning of place cell activity**

189 Data recorded on the cheeseboard maze were used for the analysis of spatial tuning of spiking
190 activity. Only data during epochs when the mouse was running faster than 5 cm/s were used.
191 Position of the animal was determined by recording LEDs on the head stage at 30 Hz using a
192 custom-made tracking software. The position and spiking data were sorted into 3 cm \times 3 cm
193 bins to generate raw maps of spike counts and occupancy. A Gaussian kernel (s.d. = 5 cm) was
194 applied for both raw maps of spike and occupancy, and a smoothed rate map was constructed
195 by dividing the smoothed spike map by the smoothed occupancy map. The smoothed rate maps
196 obtained for the pre-learning and post-learning exploration epochs were used to compute the
197 mean and peak firing rates in the maze as well as the number of place fields. A place field was
198 defined as a contiguous region of at least 72 cm² (eight bins) where the firing rate was above
199 60% of the peak rate in the maze, containing at least one bin above 80% of the peak rate in the
200 maze⁶². *Sparsity*, *spatial selectivity*, and *spatial information*⁶³ were computed from the
201 smoothed rate maps^{62,64}. Units with a peak firing rate lower than 0.4 Hz and an information
202 content lower than 0.25 bit/spike were not considered as place cells. If the information content
203 of the cell was similar ($P > 0.05$) to chance level (computed by parsing the spike train of the
204 cell and the position of the mouse – speed > 5 cm/s - into 30s blocks and shuffling these
205 “spikes” and “position” blocks 100 x relative to each other’s⁶⁴), the cell was also not a
206 considered as place cell. Only putative pyramidal cells that were defined as place cells in the
207 circular maze (start box excluded) in at least one of the two exploration epochs (pre- or post-
208 learning) were considered for analyses. Of the 1020 putative pyramidal cells 637 were
209 classified as place cells in the maze: 167 were silenced by SPW-R-triggered light pulses

210 (referred to as "silenced"), 81 were silenced with a delay after SPW-R detection (referred to as
211 "delayed"), 283 were control place cells (referred to as "control") and 106 were discarded
212 because their light-response and/or location did not meet the criteria for any of these three
213 categories (non-modulated cell on illuminated shank, undefinable response due to low firing
214 rate or increased activity during light pulses; see "Optogenetic suppression of pyramidal
215 neurons" section).

216

217 **Statistical analyses**

218 All statistical analyses were performed in Matlab (MathWorks). Number of animals and
219 number of recorded cells were similar to those generally employed in previous reports¹⁴⁻
220 ^{16,25,29,30,36,37,65}. All tests were two-tailed unless indicated. For all tests, non-parametric Mann-
221 Whitney U test, Wilcoxon's paired signed rank test and Kruskal Wallis one-way analysis of
222 variance were used. Tukey's *post-hoc* tests were performed for multiple comparisons. Analysis
223 of place cells properties (remapping, place field characteristics) was done blindly relative to the
224 cell categories these cells belonged to (control, delayed and silenced groups - approach 1 - or
225 ripple-locked or ripple-delayed groups -approach 2-). Outlier values not represented in Figure 4
226 and S8f-g were included in statistical analysis (their exclusion does not affect the conclusions).
227 Results are displayed as mean \pm SEM unless indicated otherwise.

228

229 **Quantification of spatial map stability**

230 Place map stability for individual place cells was defined by the bin-by-bin Pearson's
231 correlation coefficient between the firing rate maps of the pre- and post-learning exploration
232 epochs. Only spatial bins visited by the mouse for at least 100 ms during both epochs were
233 taken into account.

234

235 *Place field overlap*

236 Spatial bins of place fields were defined as described above. A place cell was considered to
237 have no-overlapping place fields if it displayed pre-probe and post-probe place fields that had
238 no spatial bins in common. Place cells that had place fields in one of the probe session but no

239 place fields in the other probe session were also considered as having "non-overlapping" place
240 fields.

241

242 *Population vector analysis*

243 Among all recording sessions, we identified sessions with at least 5 place cells ('ensembles') in
244 a given category (*silenced*, *control* or *delayed*) (range: 5 to 28 place cells). For each ensemble,
245 we computed the correlation value obtained for individual spatial bins between the pre-learning
246 and post-learning exploration epochs^{30,65}. The stability score corresponded to the median of
247 these per-bin correlation values obtained for a given ensemble of place cells. Only bins visited
248 by the animal longer than 100 ms during both pre-learning and post-learning exploration
249 epochs were included in this analysis. For the comparison of pairs of simultaneously recorded
250 ensembles (Fig. 6), we used a down-sampling approach in order to control for ensemble size.
251 First, the number of place cells part of the smaller ensemble of the pair (N) was determined.
252 Next, we randomly selected N cells from the larger ensemble of the pair and computed the
253 corresponding stability score as previously described. We repeated this procedure up to 100
254 times and computed the average stability score obtained from the scores of down-sampled
255 ensembles. This averaged stability score was assigned to the larger ensemble of the pair (see
256 Supplementary Fig. 6).

257

258 **Goal location representation**

259 *Probability of spiking in goal areas*

260 For each neuron, we first computed a "probability map" which indicates the probability of the
261 neuron to emit an action potential in a spatial bin of the maze per time unit. This map was
262 obtained by dividing the rate map of the neuron by the sum of the rates accumulated over all
263 visited spatial bins. From this probability map, we then added the probability values
264 corresponding to the visited spatial bins surrounding the three goal locations (circular areas of
265 5 cm radius centered on the goal wells). The resulting value was then normalized by dividing it
266 by the total number of spatial bins included in the sum. This procedure was done independently
267 for the pre-learning and the post-learning exploration epochs (see Supplementary Fig. 8a).

268 *Distance of place field to goal areas*

269 Place fields were defined as described previously. For each place field, the shortest distance
270 between its (i) edge, (ii) peak or (iii) centroid and any of the three goal locations was
271 determined. If a neuron had multiple place fields, only the minimal value was considered (ie
272 the place field closest to any goal location) (see Supplementary Fig. 8b).

273

274 **Histological processing**

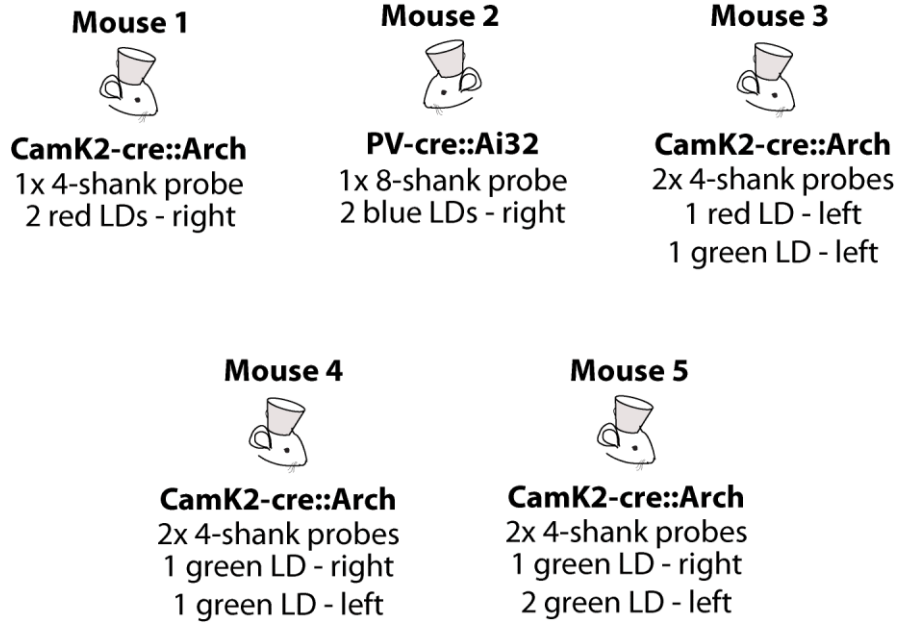
275 Mice were anesthetized with pentobarbital (100 mg/kg intraperitoneal) and perfused with
276 saline and 4% paraformaldehyde before their brains were rapidly removed. Coronal sections
277 (100 μ m) were cut on a vibratome (Leica, VT1000S) and collected in phosphate buffered
278 saline (PBS). After 3 washes in PBS (10 min each), sections were permeabilized in PBS
279 containing 0.2% Triton-X100 (PBS*) for 20 minutes. Sections were then incubated for 20 min
280 in PBS* containing DAPI (1:10000; D1306, Molecular Probes), and washed again 3 times (10
281 min each) in PBS. Sections were mounted in Fluoromount (Sigma) and imaged with a wide-
282 field fluorescence microscope (Zeiss, Axioscope).

283

Online Methods References

51. Stark, E., Koos, T. & Buzsaki, G. Diode probes for spatiotemporal optical control of multiple neurons in freely moving animals. *J Neurophysiol* **108**, 349-363, (2012).
52. Stark, E., Eichler, R., Roux, L., Fujisawa, S., Rotstein, H. G. *et al.* Inhibition-induced theta resonance in cortical circuits. *Neuron* **80**, 1263-1276, (2013).
53. Madisen, L., Mao, T., Koch, H., Zhuo, J. M., Berenyi, A. *et al.* A toolbox of Cre-dependent optogenetic transgenic mice for light-induced activation and silencing. *Nat Neurosci* **15**, 793-802, (2012).
54. Chow, B. Y., Han, X., Dobry, A. S., Qian, X., Chuong, A. S. *et al.* High-performance genetically targetable optical neural silencing by light-driven proton pumps. *Nature* **463**, 98-102, (2010).
55. Boyden, E. S., Zhang, F., Bamberg, E., Nagel, G. & Deisseroth, K. Millisecond-timescale, genetically targeted optical control of neural activity. *Nat Neurosci* **8**, 1263-1268, (2005).
56. Tsien, J. Z., Chen, D. F., Gerber, D., Tom, C., Mercer, E. H. *et al.* Subregion- and cell type-restricted gene knockout in mouse brain. *Cell* **87**, 1317-1326, (1996).
57. Hippenmeyer, S., Vrieseling, E., Sigrist, M., Portmann, T., Laengle, C. *et al.* A developmental switch in the response of DRG neurons to ETS transcription factor signaling. *PLoS Biol* **3**, e159, (2005).
58. Berenyi, A., Somogyvari, Z., Nagy, A. J., Roux, L., Long, J. D. *et al.* Large-scale, high-density (up to 512 channels) recording of local circuits in behaving animals. *J Neurophysiol* **111**, 1132-1149, (2014).
59. Kesner, R. P., Farnsworth, G. & Kametani, H. Role of parietal cortex and hippocampus in representing spatial information. *Cereb Cortex* **1**, 367-373, (1991).
60. Harris, K. D., Henze, D. A., Csicsvari, J., Hirase, H. & Buzsaki, G. Accuracy of tetrode spike separation as determined by simultaneous intracellular and extracellular measurements. *J Neurophysiol* **84**, 401-414, (2000).
61. Hazan, L., Zugaro, M. & Buzsaki, G. Klusters, NeuroScope, NDManager: a free software suite for neurophysiological data processing and visualization. *J Neurosci Methods* **155**, 207-216, (2006).
62. Mizuseki, K., Royer, S., Diba, K. & Buzsaki, G. Activity dynamics and behavioral correlates of CA3 and CA1 hippocampal pyramidal neurons. *Hippocampus* **22**, 1659-1680, (2012).
63. Skaggs, W. E., McNaughton, B. L., K.M., G. & E.J., M. in *Advances in Neural Information Processing Systems* Vol. 5 (eds S.J. Hanson, J.D. Cowan, & C.L. Giles) 1030-1037 (Morgan Kaufmann, 1993).
64. Markus, E. J., Barnes, C. A., McNaughton, B. L., Gladden, V. L. & Skaggs, W. E. Spatial information content and reliability of hippocampal CA1 neurons: effects of visual input. *Hippocampus* **4**, 410-421, (1994).

65. Leutgeb, J. K., Leutgeb, S., Treves, A., Meyer, R., Barnes, C. A. *et al.* Progressive transformation of hippocampal neuronal representations in "morphed" environments. *Neuron* **48**, 345-358, (2005).



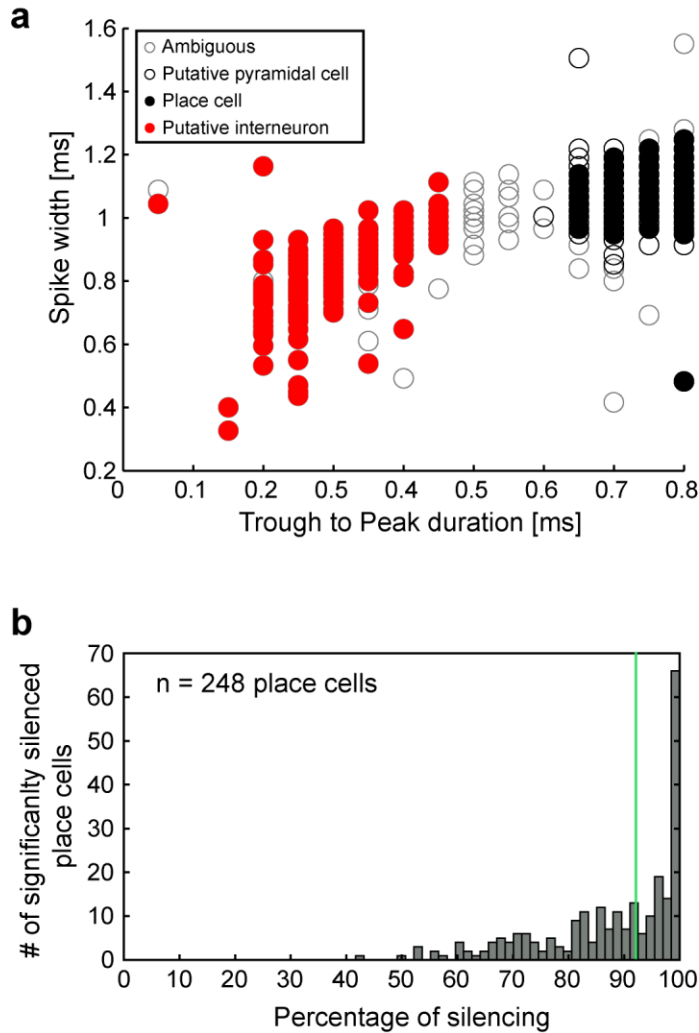
Supplementary Figure 1: Summary of the transgenic mice used in this study with their recording and optogenetic equipment. In four mice, cre-dependent expression of the hyperpolarizing opsin Arch in pyramidal cells was achieved via the expression of Cre recombinase under the CamKIIalpha promoter. In one mouse, cre-dependent expression of the depolarizing opsin ChR2 (Ai32) in inhibitory PV positive cells was achieved via the expression of Cre recombinase under the PV promoter. Four or 8-shank silicon probes equipped with laser diode (LD) coupled optical fibers were implanted uni- or bilaterally (right and/or left hemisphere)⁵¹.

Mouse ID	Session ID	Control place cells	Delayed place cells	Silenced place cells	Sessions with pair of ensembles ¹	Number of PYR cells	Excluded PYR ²	Control PYR cells	Delayed PYR cells	Silenced PYR cells	Number of trials
1	session 1	3	0	2		13	5	6	0	2	52
	session 2	5	0	0		12	4	7	0	1	49
2	session 1	5	0	10	•	28	3	8	0	17	54
	session 2	5	0	6	•	29	9	10	0	10	60
	session 3	9	0	16	•	47	8	9	0	30	55
3	session 1	2	0	0		30	4	22	0	4	34
	session 2	6	2	0		35	6	23	6	0	38
	session 3	5	0	5	•	31	1	18	0	12	45
	session 4	2	3	0		22	5	5	12	0	60
	session 5	2	0	0		21	3	18	0	0	50
	session 6	13	0	8	•	38	3	23	0	12	56
4	session 1	18	0	13	•	41	1	25	0	15	50
	session 2	28	0	13	•	59	7	33	0	19	48
	session 3	18	11	0	•	44	6	23	15	0	51
	session 4	5	0	0		44	4	35	4	1	41
	session 5	26	2	6	•	50	9	30	3	8	49
	session 6	20	0	6	•	45	6	24	0	15	50
	session 7	26	13	0	•	51	8	29	14	0	51
	session 8	6	6	3	•	33	4	12	11	6	50
	session 9	11	2	5	•	31	4	15	3	9	50
5	session 1	0	1	8		14	2	1	2	9	36
	session 2	6	4	6	•	23	1	7	5	10	42
	session 3	10	0	16	•	54	11	15	0	28	29
	session 4	12	22	0	•	55	13	13	29	0	42
	session 5	13	0	7	•	35	8	16	0	11	43
	session 6	8	6	0	•	22	2	11	9	0	45
	session 7	7	0	23	•	47	8	7	0	32	50
	session 8	5	9	0	•	24	1	7	16	0	46
	session 9	7	0	14	•	42	12	8	0	22	46
Total		283	81	167		1020	158	460	129	273	1372

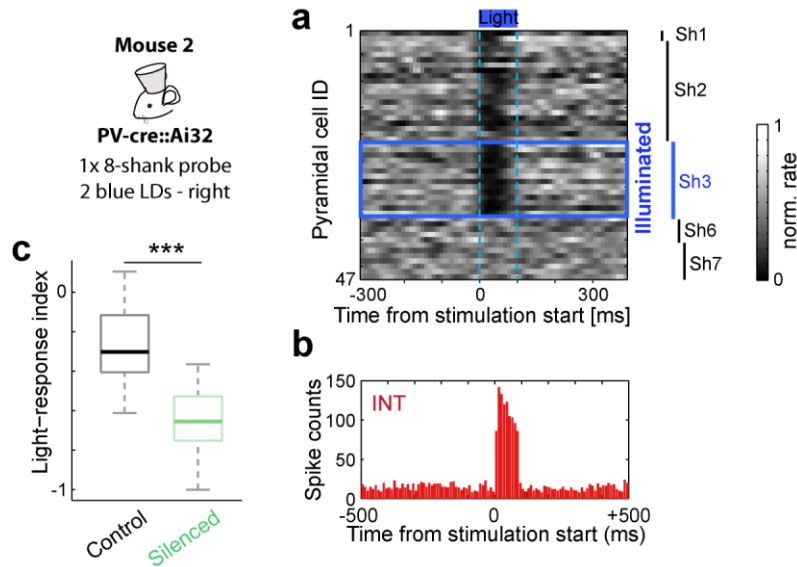
Supplementary Table 1: Summary of the number of place cells from each group recorded in each session and number of learning trials. Highlighted in color boxes are the sessions used for population vector analysis of Figure 5 (at least 5 place cells simultaneously recorded).

¹ Sessions used for population vector analysis of simultaneously recorded ensembles (see Fig. 6)

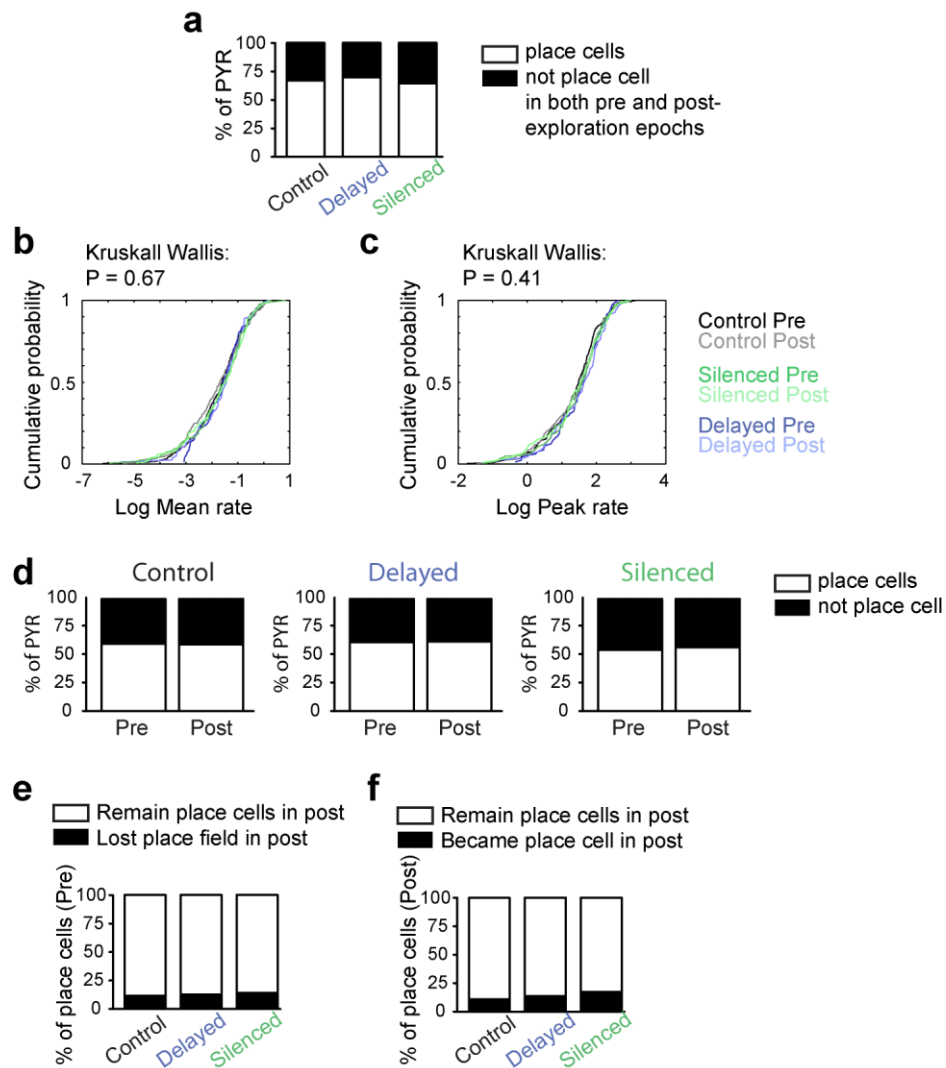
² Excluded because of undefined light response, because the cell showed increased firing during light pulses, or because it was located on the illuminated shank but not modulated by light (excluded control cell; see online Methods)



Supplementary Figure 2: Details of unit classification. **(a)** Distribution of the spike waveform features used to distinguish putative pyramidal cells (PYR) and interneurons (see ref [52], online Methods). **(b)** Distribution of the silenced ($P < 0.05$, Wilcoxon’s paired signed rank test) place cells used in our study (“*silenced*” and “*delayed*” categories) according to their response to light pulses. Percentage of silencing is computed by comparing the mean rate during the 100 ms light pulses of the response mapping and the mean rate measured during 100ms intervals starting 1 s before the pulses (baseline rate). The median silencing value (92.2%) is shown by a green line. Most cells show more than 50% silencing (87.5 ± 0.8 %; mean \pm SEM; range 40-100%).

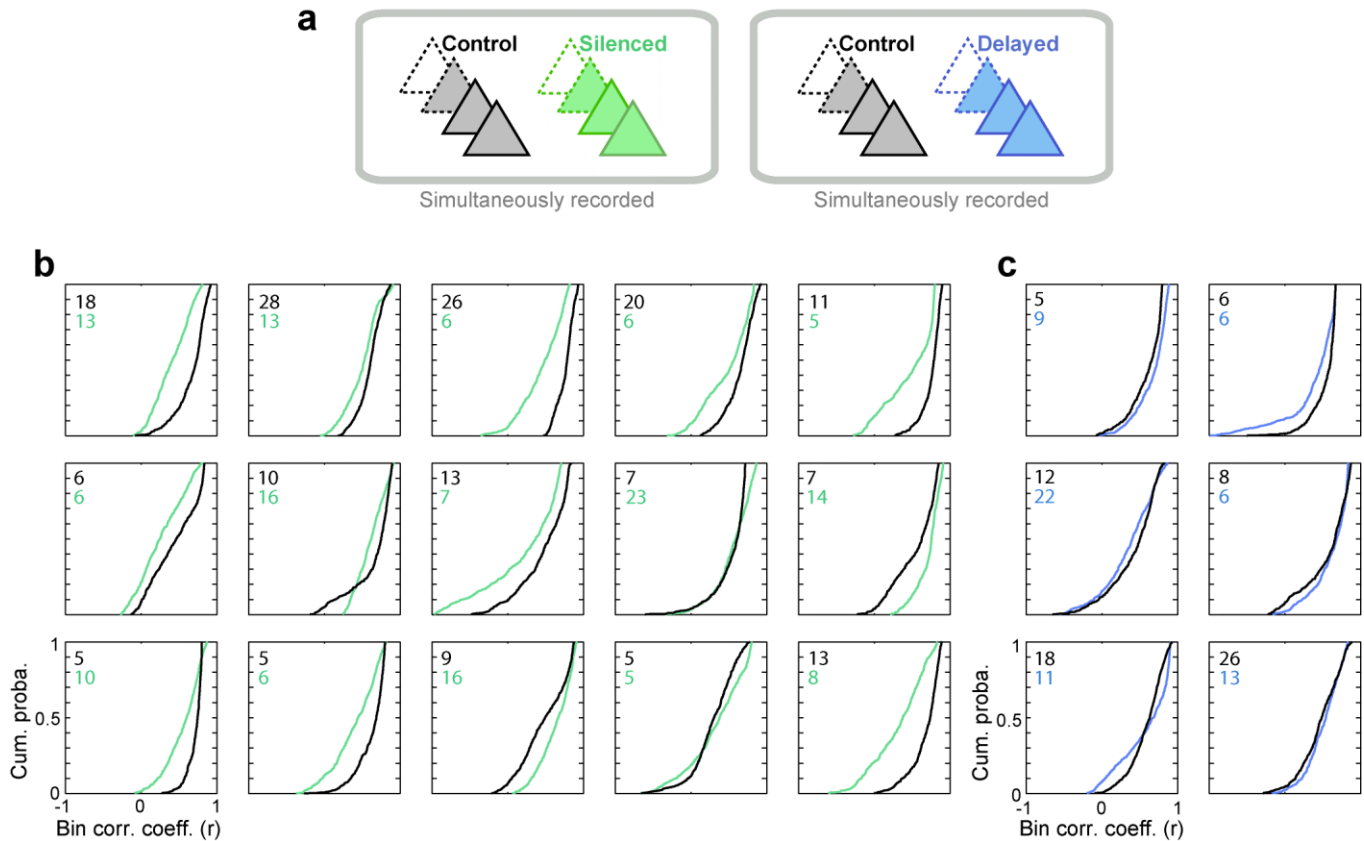


Supplementary Figure 3: Indirect silencing of pyramidal cells by optogenetic activation of inhibitory PV cells in the PV-cre::ChR2 mouse. **(a)** Peristimulus response of 47 simultaneously recorded pyramidal cells. The position of the units on the 8-shank silicon probe is indicated on the right. Blue light was delivered on shank 3 (Sh3; blue box). Consistent with previous observations⁵², a weak non-local silencing is also observed for neurons recorded on the adjacent shank (200 μm from illuminated shank) but not on more distant shanks ($\geq 400 \mu\text{m}$ from the illuminated shank). More pyramidal cells are silenced than with direct Arch-suppression of pyramidal neurons possibly because axons collaterals of CA1 PV interneurons cover a larger region. **(b)** Peristimulus histogram for a light-activated PV-positive neuron. **(c)** Quantification of light-response indices for control and silenced place cells recorded in the PV-cre::ChR2 mouse. Indices: -0.25 ± 0.05 and -0.64 ± 0.03 for *control* and *silenced* pyramidal cells, respectively. Mann-Whitney U test: $***P = 1.7 \times 10^{-7}$; $n = 19$ and $n = 32$ *control* and *silenced* pyramidal cells, respectively).

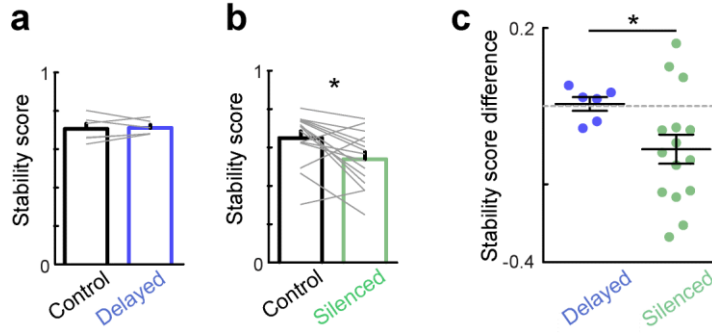


Supplementary Figure 4: Silencing pyramidal cells during SPW-Rs does not affect their firing rates or ability to code for space. **(a)** Proportion of place cells identified among *control*, *delayed* and *silenced* pyramidal cells - PYR - (308 out of 460; 90 out of 129; 176 out of 273 PYR for *control*, *delayed* and *silenced* groups, respectively). Inclusion of place cell had to meet our criteria (see online Methods) in at least one of the exploration epochs (pre- or post-learning). Place cells in the start box are included. χ^2 test: P = 0.56. **(b)** The mean firing rates of *control*, *delayed* and *silenced* place cells are similar between pre- or post-learning exploration epochs (*control*: 0.27 ± 0.01 and 0.27 ± 0.02 spk/s; *delayed*: 0.28 ± 0.03 and 0.29 ± 0.03 spk/s; *silenced*: 0.30 ± 0.02 and 0.29 ± 0.02 spk/s for pre and post, respectively; Kruskal Wallis test, P = 0.67; n

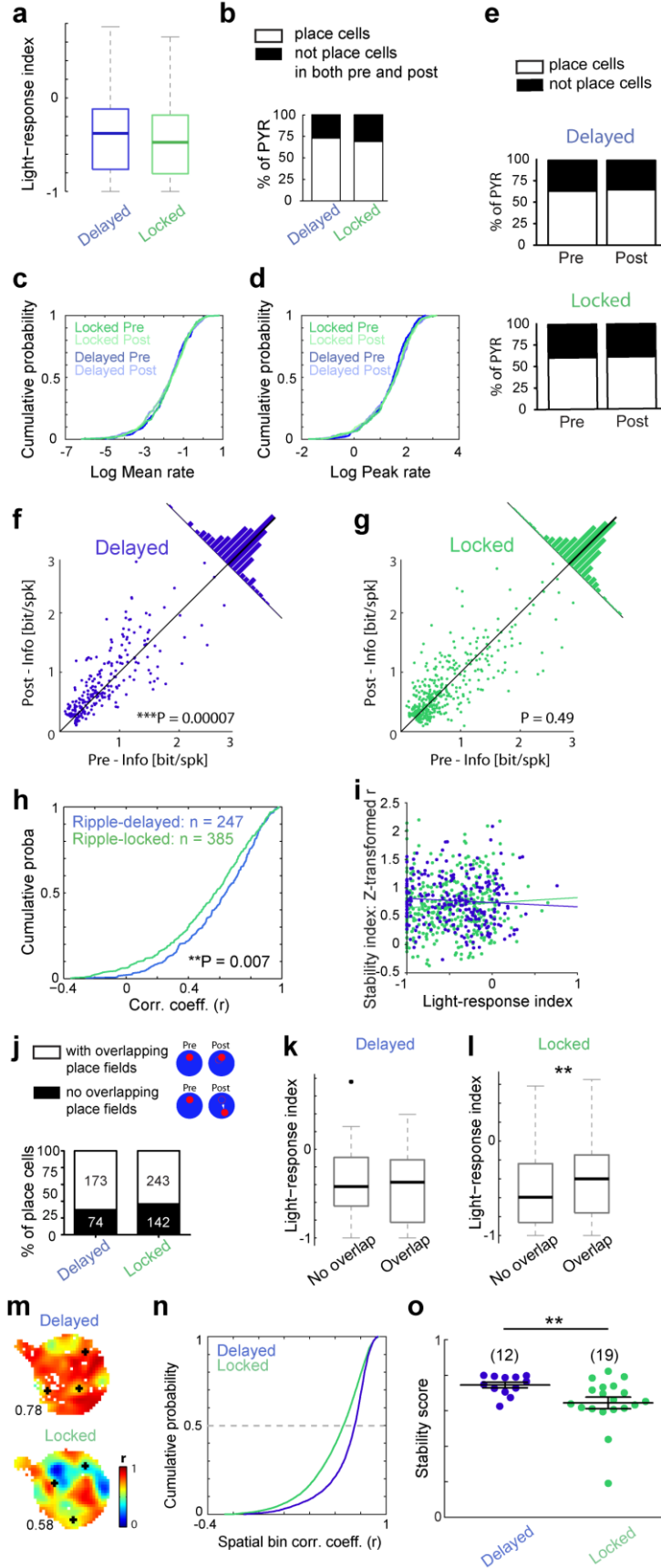
= 283; 81; 167 place cells for *control*, *delayed* and *silenced* groups, respectively). **(c)** The peak firing rates of *control*, *delayed* and *silenced* place cells are similar between pre- or post-learning exploration epochs (*control*: 5.01 ± 0.21 and 5.28 ± 0.22 spk/s; *delayed*: 5.45 ± 0.35 and 5.88 ± 0.43 spk/s; *silenced*: 5.43 ± 0.29 and 5.35 ± 0.28 spk/s for pre and post, respectively; Kruskal Wallis test, $P = 0.41$). Both mean and peak firing rates were obtained from the rate maps for each exploration epochs (pre and post-learning). **(d)** The proportion of place cells identified among *control*, *delayed* and *silenced* pyramidal cells is similar between the pre- and post-learning exploration epochs. $n = 460, 129$ and 273 PYR for *control*, *delayed* and *silenced* groups, respectively. χ^2 tests: $P = 0.84$, $P = 0.90$ and $p = 0.61$ for *control*, *delayed* and *silenced* groups, respectively. The fact that the proportion of place cells is identical between the pre- and post-learning exploration epochs in the *silenced* group indicates that SPW-R silencing does not impact the ability of pyramidal cells to code for their environment. **(e)** Some neurons identified as place cells in the pre-learning exploration did not meet the criteria for place cell in the post-learning exploration epoch. The proportion of these neurons was similar among the three groups indicating that SPW-R silencing does not induce place cell disappearance (χ^2 test, $P = 0.76$; $n = 276, 79$ and 149 place cells identified in the pre-learning exploration epoch for *control*, *delayed* and *silenced* groups, respectively). **(f)** Some of the neurons identified as place cells in the post-exploration were not place cells in the pre-learning exploration epoch. The proportion of these neurons was similar in the three groups indicating that SPW-R-silencing does not result in additional place cell formation (χ^2 test, $p = 0.13$; $n = 273, 80$ and 155 place cells identified in the post-learning exploration epoch for *control*, *delayed* and *silenced* groups, respectively; place cells with place field in start box are included).



Supplementary Figure 5: Within-session comparison of the stability of simultaneously recorded place cell ensembles. **(a)** Schematic illustrating the method used for within-session comparison of pairs of place cell ensembles. One ensemble is composed of at least 5 place cells simultaneously recorded in the same session. **(b)** Cumulative distribution of the population correlation values across spatial bins for pairs of *control* and *silenced* place cell ensembles recorded in the individual sessions (each panel corresponds to one pair/session). Top left: number of place cells part of the ensembles. **(c)** Cumulative distribution of the population correlation values across spatial bins for pairs of *control* and *delayed* ensembles of place cells recorded in the individual sessions.

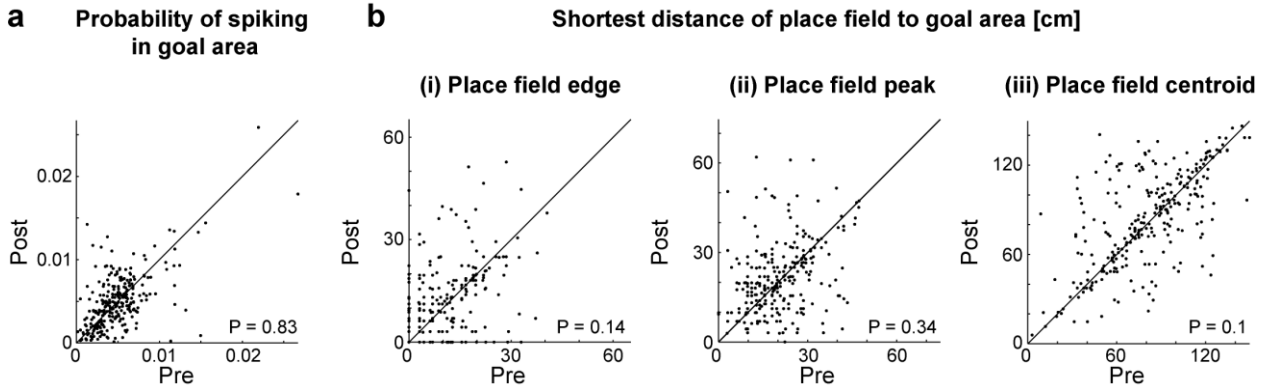


Supplementary Figure 6: SPW-R silenced place cell ensembles show non-stabilized spatial representation as compared to simultaneously recorded control ensembles after controlling for ensemble size. **(a, b)** Comparison of pairs of simultaneously recorded ensembles was conducted after randomly downsampling (up to 100 times) the larger ensemble of the pair to match the number of cells in the smaller ensemble of the pair (see online Methods). **(a)** Ensembles of *delayed* place cells are similar to their matching *control* ensembles with equated ensemble sizes (score = 0.71 ± 0.03 and 0.71 ± 0.02 for *control* and *delayed* ensembles, respectively; Wilcoxon's signed rank test, $P = 0.84$, $n = 6$ pairs). **(b)** In contrast, ensembles of *silenced* place cells show lower stability scores compared to their matching *control* ensembles from the same session with equated ensemble sizes (score = 0.65 ± 0.03 and 0.54 ± 0.04 for *control* and *silenced* ensembles, respectively; $*P = 0.02$, $n = 15$ pairs). **(c)** Within-session differences between the stability scores of optogenetically manipulated ensembles and their matching control ensembles (0.005 ± 0.02 for *delayed-control* pairs and -0.11 ± 0.04 for *silenced-control* pairs). Mann-Whitney U test: $*P = 0.047$.



Supplementary Figure 7: Comparison of place cells recorded in *ripple-locked* and *ripple-delayed* categories supports a role for SPW-Rs in place field stabilization and refinement. **(a)** Place cells from both groups have similar light response indices (index = -0.42 ± 0.02 and -0.48 ± 0.02 , for “*ripple-delayed*” and “*ripple-locked*” place cells with identifiable light-response; $n = 240$ and 377 ; Mann-Whitney U test, $P = 0.07$). **(b)** Proportion of place cells identified among *ripple-delayed* and *ripple-locked* pyramidal cells - PYR - (247 out of 369 ; 385 out of 601 PYR for *ripple-delayed* and *ripple-locked* groups, respectively). Place cells coding in the start box are included. χ^2 test: $P = 0.22$. **(c)** The mean firing rates of *ripple-delayed* and *ripple-locked* place cells are similar between pre- and post-learning exploration epochs (*ripple-delayed*: 0.27 ± 0.02 spk/s for both pre and post; *ripple-locked*: 0.28 ± 0.01 and 0.27 ± 0.01 spk/s for pre and post, respectively; Kruskal Wallis test, $P = 0.92$; $n = 247$ and 385 place cells for *ripple-delayed* and *ripple-locked* groups, respectively). **(d)** The peak firing rates of *ripple-delayed* and *ripple-locked* place cells are similar between pre- and post-learning exploration epochs (*ripple-delayed*: 4.90 ± 0.20 and 5.40 ± 0.23 spk/s; *ripple-locked*: 5.34 ± 0.19 and 5.34 ± 0.19 spk/s for pre and post, respectively; Kruskal Wallis test, $P = 0.59$). Both mean and peak firing rates were obtained from the rate maps for each exploration epochs (pre- and post-learning). **(e)** The proportion of place cells identified among *ripple-delayed* and *ripple-locked* PYR cells is similar between the pre- and post-learning exploration epoch (χ^2 tests: $P = 0.64$ and $P = 0.86$ for *ripple-delayed* and *ripple-locked* groups, respectively). **(f-g)** Distribution of information content values carried by place cells before and after learning (during pre- and post-learning exploration epochs). The information content of *ripple-locked* place cells remained similar in the pre- and post-learning exploration epochs (Wilcoxon’s paired signed rank test: $P = 0.49$; $n = 385$ place cells) while the control *ripple-delayed* place cells showed an increased information content ($***P = 6.6 \times 10^{-5}$, $n = 247$ place cells). Two outlier values in the *ripple-locked* group and one in the *ripple-delayed* group are not displayed but included in the statistical analyses (their exclusion does not affect the conclusions). **(h)** Cumulative distributions of the Pearson correlation coefficients (r) obtained for individual place cells in the two groups ($r = 0.60 \pm 0.02$ and 0.53 ± 0.02 for *ripple-delayed* and *ripple-locked* groups, respectively; Mann-Whitney U test: $**P = 0.007$). Results were similar with Spearman's correlation coefficients ($**P = 0.006$). **(i)** No linear correlation (R) was present between the light response index and the pre-post correlation value measured for individual place cells in the *ripple-locked* (green) and *ripple-*

delayed (blue) paradigms ($R = 0.07$, $P = 0.2$ for *ripple-locked* units; $R = -0.09$, $P = 0.2$ for *ripple-delayed* units; Pearson's test). **(j)** Proportions of place cells with shifting fields (no overlapping place fields, back) or overlapping place fields (white) in the two groups of place cells. The number of cells in each category is indicated on the bars. χ^2 test: $P = 0.07$. **(k)** Both place cells with shifting fields ($n = 74$) and non-shifting cells ($n = 166$) have similar light response indices in the *ripple-delayed* group (indices: -0.39 ± 0.04 and -0.43 ± 0.03 ; Mann-Whitney U test, $P = 0.58$). **(l)** Place cells with shifting fields ($n = 140$) have lower light response indices than non-shifting place cells ($n = 237$) in the *ripple-locked* group (indices: -0.54 ± 0.03 and -0.44 ± 0.02 ; $**P = 0.005$). Only cells with identifiable light-responses are included. **(m)** Examples of correlation maps obtained for *ripple-delayed* and *ripple-locked* place cell ensembles. The population correlation value, computed for individual spatial bins (r), is color coded. The stability score is indicated on the left of each map (black). Goal locations are shown with black crosses. **(n)** Cumulative distributions of the correlation values accumulated for all ensembles of place cells from the two groups. **(o)** Ensembles of *ripple-locked* place cells showed reduced stability as compared to control *ripple-delayed* ensembles. Stability scores: 0.75 ± 0.02 and 0.64 ± 0.03 for *ripple-delayed* and *ripple-locked* ensembles, respectively; Mann-Whitney U test: $**P = 0.009$. $n = 12$ *ripple-delayed* and $n = 19$ *ripple-locked* place cell ensembles.



Supplementary Figure 8: Goal location representation before and after learning. **(a)** The probability of place cells to spike in goal areas (15 cm diameter region centered on reward locations used during the learning task) is similar in the pre- and post-learning exploration epochs (Wilcoxon’s paired signed rank test, $P = 0.83$; $n = 283$ control place cells). **(b)** The distance of place field(s) to reward location is comparable between the pre and post-learning exploration epochs, whether place field edge ($P = 0.14$), peak ($P = 0.34$) or centroid ($P = 0.10$) is considered. Edge: 9.82 ± 0.53 and 9.82 ± 0.53 cm; peak: 20.45 ± 0.61 and 21.24 ± 0.71 cm; centroid: 80.85 ± 1.84 and 83.99 ± 1.94 cm for pre and post, respectively. $n = 272$ control place cells with place fields in both pre- and post-exploration epochs. These findings demonstrate the lack of specific goal area-related remapping of place cells.